



Measurements within the Pacific-Indian oceans throughflow region

M. FIEUX,* C. ANDRIÉ,* P. DELECLUSE,* A. G. ILAHUDE,†
 A. KARTAVTSEFF,* F. MANTISI,‡ R. MOLCARD* and J. C. SWALLOW§

(Received 15 September 1990; in revised form 26 April 1993; accepted 30 April 1993)

Abstract—Two hydrographic (θ , S , O_2) and trichlorofluoromethane (F-11) sections were carried out between the Australian continental shelf and Indonesia, in August 1989, on board the R.V. *Marion Dufresne*. The sections lie in the easternmost part of the Indian Ocean where the throughflow between the Pacific Ocean and the Indian Ocean emerges. They allow us to describe the features of the water-property and circulation fields of the throughflow at its entrance in the Indian Ocean. Between the Australian continental shelf and Bali, the Subtropical and Central waters are separated from the waters of the Indonesian seas by a sharp hydrological front, located around 13°30 S, below the thermocline down to 700 m. Near the coast of Bali, upwelling occurs in the near-surface layer under the effect of the southeast monsoon; at depth, between 300 m to more than 800 m, a water mass of northern Indian Ocean origin was present. From the characteristics of the bottom water found in the Lombok basin, the maximum depth of the Java ridge which separates the Lombok basin from the Northwest Australian basin lies around 3650 m. Off Sumba, Savu, Roti and Timor channels a core of low salinity and high oxygen content near-surface water was found in the axis of each channel, which suggests strong currents from the interior Indonesian seas towards the Indian Ocean. The entrance of the deep water flowing in the opposite direction, from the Indian Ocean to the Timor basin, was marked below 1400 m to the sill depth, through an increase of salinity and oxygen content. The flow reversal, observed briefly by a Pegasus direct current profiler in the Timor strait, was located at 1200 m depth.

During the southeast monsoon, the net (geostrophic + Ekman) transport calculated on the section Australia-Bali give an estimate of the throughflow between 0 and 500 m of $22 \pm 4 \times 10^6 \text{ m}^3 \text{ s}^{-1}$ towards the Indian Ocean, with a concentration of the transport in the upper layers ($19 \times 10^6 \text{ m}^3 \text{ s}^{-1}$ in 0-200 m) and near the Indonesian coast, north of 13°30 S. In this region of intense mixing, attempts to make a salinity budget were inconclusive but did not imply any reduction in estimated throughflow transport. Below 500 m the net transport is of the order of the uncertainty. The total estimated transport (0-1900 dbar, deepest sill depth) is $18.6 \times 10^6 \text{ m}^3 \text{ s}^{-1}$ (± 7) with a mean temperature of 23°C and a mean salinity of 34.0 psu (but may be as large as $23 \times 10^6 \text{ m}^3 \text{ s}^{-1}$, with mean temperature of 20°C and mean salinity of 34.1 psu).

1. INTRODUCTION

THE Indonesian seas are located between the Asian mainland in the northern hemisphere and the Australian continent in the southern hemisphere. Due to this particular location,

*LODYC, CNRS/ORSTOM/Université Paris 6, case 100, 4 Place Jussieu, 75252 Paris cedex 05, France.

†LIPI, Jl. Pasir Putih 1, Ancol Timur, P.O. Box 580, Jakarta, 11001, Indonesia.

‡LPCM, Université Paris 6, T.24,5 ét., 4 Place Jussieu, 75252 Paris cedex 05, France.

§Heath Cottage, Drakewalls, Gunnislake, Cornwall, U.K.

ORSTOM Documentation



010000374

1091

O.R.S.T.O.M. Fonds Documentaire

N° : 42 327

Cote : B Ex 1

14 SEP. 1995

the dominant atmospheric process over the region is a characteristic monsoon circulation associated to an intense convective activity. In April–May a low pressure center develops over the Asian mainland and a high pressure center over the Australian continent. This distribution induces a dry eastern monsoon over Indonesia, stronger and longer (June–October) than the western monsoon. In October–November, the atmospheric pressure gradient weakens and brings a transition period with weak and variable winds. During the northern hemisphere winter, a high pressure center grows over the Asian heights and a low pressure center over the Australian continent. It induces a wet western monsoon over the Indonesian seas (December–March). The air masses coming from the Indian Ocean are loaded with humidity which they discharge over the hilly Indonesian region. The intense rains are among the highest in the world and can reach 2–3 m year⁻¹. In March, the Asiatic high decreases and the western monsoon weakens, giving way to another transition period which often lasts into April.

Over the equatorial Pacific ocean, the southeast trade winds blow during all normal years (during El Niño years westerly winds can blow in the western Pacific). These easterly winds pile up the warm surface waters on the western side of the Pacific ocean, i.e. towards Indonesia (to a lesser extent, on the Indian Ocean side, westerly winds blowing at the equator during the transition periods do the same). This is why this region of the “maritime continent”, between the eastern Indian Ocean and the western Pacific ocean, represents the largest heat reservoir of the global ocean. Consequently, large exchanges take place with the overlying atmosphere, developing the most intense atmospheric convective activity of the globe. Small anomalies of temperature in this area of high sea surface temperature ($T > 28^{\circ}\text{C}$) modify the heat flux towards the atmosphere and can have large climatological effects, locally and globally, as demonstrated by the theoretical studies on sensitivity of an atmospheric global circulation model (PALMER and MANSFIELD, 1986).

The western boundary of the tropical Pacific is “leaky”, and Pacific water can pass through the Indonesian archipelago into the Indian Ocean. This region presents one of the most complex structure on earth. Its topography is very chaotic with thousands of islands (high volcanoes or coral islands) subdividing the region into many seas, deep trenches, continental shelves, deep basins and numerous sills connecting the seas. The different passages along the Sunda are through which the Pacific waters can reach the Indian Ocean have increasing depths from northwest to southeast: Malacca, Sunda and Bali straits are shallower than 70 m. The deep straits important for the throughflow, besides Lombok strait (which has been studied by MURRAY and ARIEF, 1988), are between the islands of Flores, Sumba, Savu, Roti (extension of Timor) and the continental shelf of Australia (Figs 1 and 2).

Piled up by the southeast trade winds throughout the year, the sea level is higher at the western Pacific boundary than in the eastern Indian Ocean. This pressure gradient sets up a general flow predominantly towards the Indian Ocean (WYRTKI, 1987). Consequently, the waters of the Indonesian seas, as a whole, are principally an extension of the Pacific ocean waters. Property distributions (e.g. salinity) show that, above 1000 m, a wedge of water of mainly Pacific origin spreads from the Indonesian seas westward across the entire Indian Ocean (WYRTKI, 1971). This throughflow is supposed to represent one of the two interocean links of the warm water route, the upper part of the global scale oceanic cell in which the descending branch is in the region of formation of the North Atlantic Deep Water (GORDON, 1986).

Recent modelling studies confirm the importance of this throughflow and the conse-

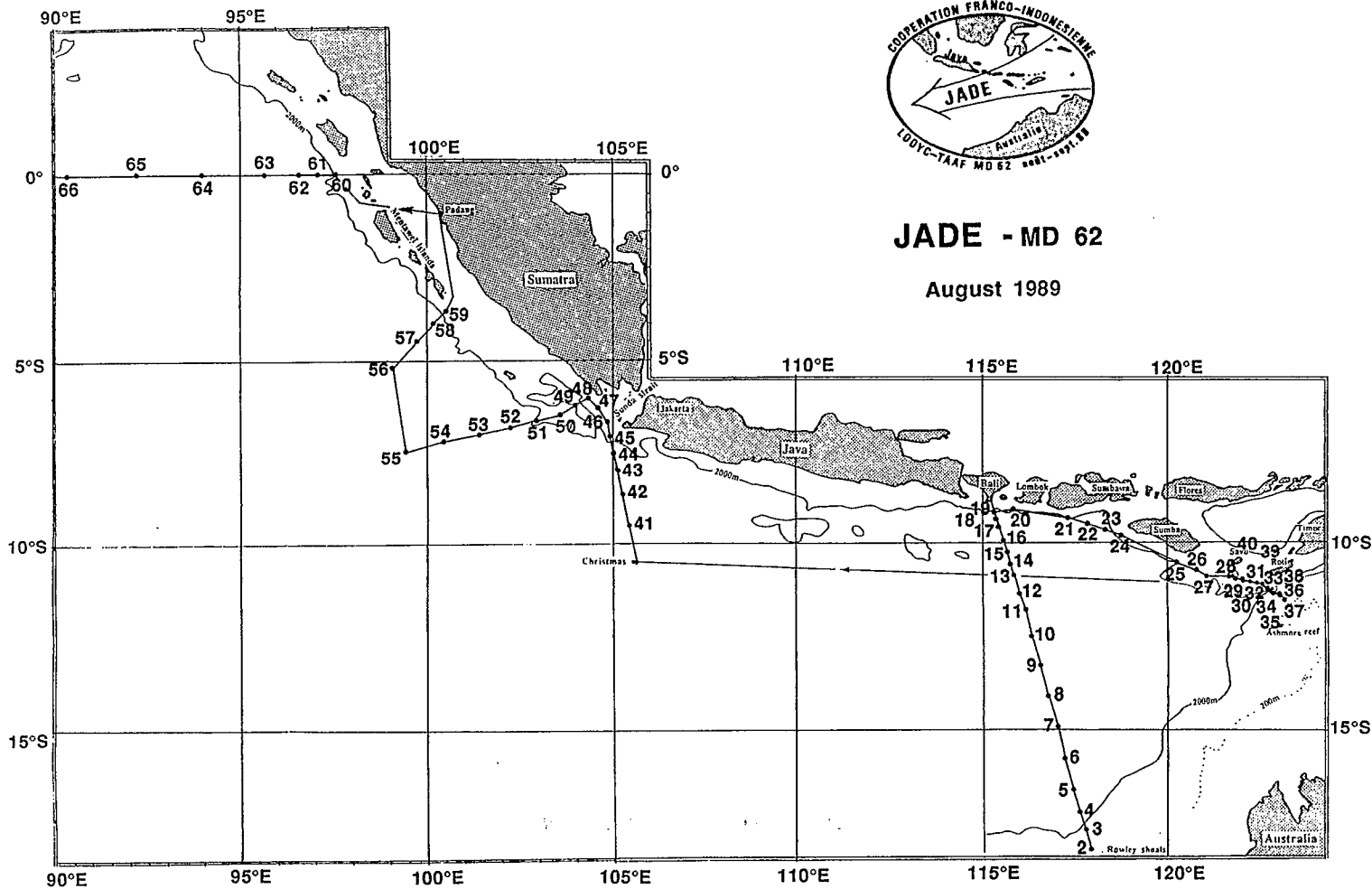


Fig. 1. Locations of the JADE stations.

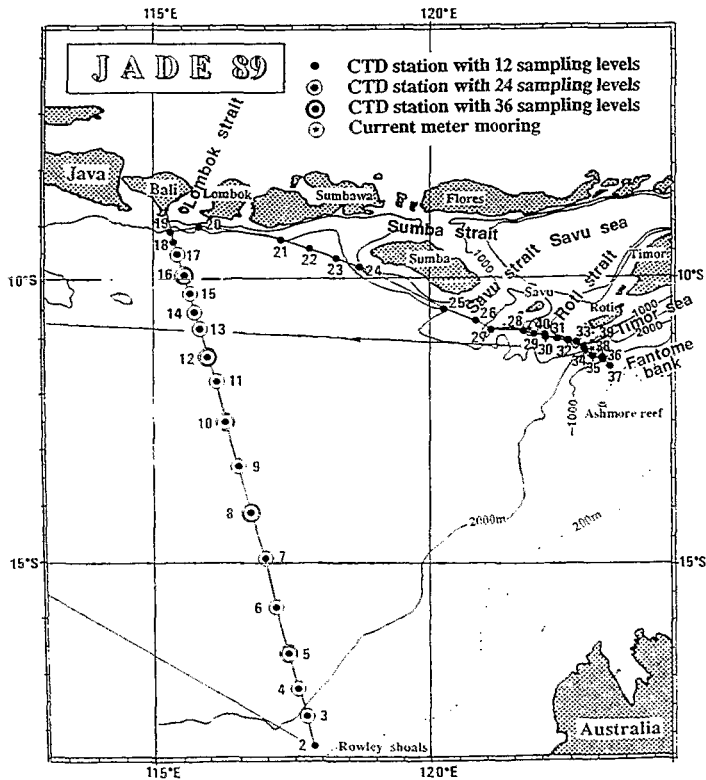


Fig. 2. Location of the stations in the throughflow.

quent heat transport (COX, 1982; KINDLE *et al.*, 1989; SEMTNER and CHERVIN, 1988). For example, it has been suggested that if this connection were closed, the temperature west of Australia would decrease by several degrees in the upper 300 m and the temperature of the equatorial Pacific would tend to increase (GODFREY and GOLDING, 1981; GODFREY and WEAVER, submitted). The Leeuwin current on the western coast of Australia, which flows in the opposite direction to the two other eastern boundary currents in the southern Atlantic and Pacific oceans, the Benguela and the Peru–Chile currents, brings warm waters from the north. Different estimates of the magnitude of the throughflow, by various indirect methods and for different seasons, vary from 1 to 18 Sv towards the Indian Ocean (WYRTKI, 1961; GODFREY and GOLDING, 1981; COX, 1982; PIOLA and GORDON, 1984; FINE, 1985; FU, 1986; GORDON, 1986; KINDLE *et al.*, 1987; MURRAY and ARIEF, 1988; SEMTNER and CHERVIN, 1988; TOOLE *et al.*, 1988; KINDLE *et al.*, 1989). The only direct long term current measurements were made in one passage south of Makassar strait, the Lombok strait in 1985 (MURRAY and ARIEF, 1988; MURRAY *et al.*, 1990); they gave an annual mean of 1.8 Sv towards the Indian Ocean with strong seasonal variability, up to 4 Sv during the southeast monsoon.

In order to estimate the Pacific–Indian throughflow during the eastern and western monsoons (in August and February), the JADE (Java Australia Dynamic Experiment) programme has been set up in cooperation with Indonesian scientists. It includes the determination of the characteristics of the water masses of the whole water column

together with some transient tracers measurements. The area studied is at the southern entrances of the Savu and Timor seas and across the easternmost basin of the Indian Ocean, between the Australian continental shelf and Bali, which comprises all the water coming through the deep Indonesian passages from the Pacific Ocean. This co-project between Indonesia and France started with the JADE 89 cruise on board the R.V. *Marion Dufresne* of the Terres Australes et Antarctiques Françaises, from 30 July to 9 September 1989. The hydrographic observations carried out in August 89 give the characteristics induced by the eastern monsoon. The ship track and the location of the stations are indicated on Fig. 1. The section at the outflow of the Indonesian seas is located 12 miles off the line Lombok-Sumba-Dana-Roti, outside the territorial waters (Fig. 2). This section gives the characteristics of the water masses coming from the western Pacific ocean through the Indonesian passages. The other section runs from the Australian continental shelf to Indonesia cutting the outflows around 116°E.

Here sampling and analytical methods are presented. Then the water mass characteristics, including F-11 data, are described. An estimation of the transports are given through geostrophic calculations.

2. SAMPLING AND ANALYTICAL METHODS

Along the track Colombo-Bali-Christmas-Padang-Colombo, 65 hydrographic stations were occupied (Fig. 1) with a Neil Brown Mark III CTDO₂ equipped with a 12-12 l bottle G.O. rosette sampler. Eighteen CTD stations were occupied between the continental shelf of Australia (Rowley shoals) and the coast of Indonesia (off Bali). The intervals between stations varied from 95 km, in the deep part, to 20 km near Bali (Fig. 2). Because of time constraints due to a previous fire on board, only five of the stations were three-cast stations (0-600 m, 0-2200 m, 0-bottom), 10 were two-cast stations (0-600 m, 0-2200 m or 0-bottom) and three were one-cast stations (0-bottom). Eleven stations sampled the whole water column. The two CTD stations near Bali were difficult to handle because of the very strong current shear in the surface layer together with strong winds (Sta. 18 reached only 445 db). Twenty-one one-cast CTD stations were done down to the bottom between Bali and Ashmore reef to get the water masses characteristics at their entrance in the Indian Ocean.

The r.m.s. of the differences between the salinity measured by the Neil Brown CTD and the measurements made on board for the calibration with a Guildline salinometer (which has itself an uncertainty of 0.003 psu) is ± 0.0035 psu (per standard unit of the 1978 Practical Salinity Scale) and is ± 0.023 ml l⁻¹, for the oxygen values (with an uncertainty of the method of 0.02 ml l⁻¹). The temperature and the pressure sensors have been calibrated in Brest Center after the cruise. The r.m.s. of the differences between the temperature given by the CTD and the calibration data is = 0.0002°C, but the temperature reference has an absolute uncertainty of ± 0.003 °C. The r.m.s. of the differences between the pressure given by the CTD and the calibration data is 0.26 dbar but the absolute uncertainty is ± 5 dbar (FIEUX *et al.*, 1990). The potential density anomaly (σ_θ in mg cm⁻³) deduced from the potential temperature and the salinity was done with the EOS 80 definition. Adequate samples were collected for the following analyses: salinity, F-11, tritium, helium-2, carbon-14, oxygen, TCO₂ and total alkalinity, phosphate, nitrate and silicate. Surface temperature, salinity and pH were recorded continuously on board as well as pCO₂ in the air and in surface water. Meteorological parameters were measured every

hour. Analysis of F-11 was carried out by gas chromatography and electron capture detection (BULLISTER and WEISS, 1988; MANTISI, 1989), calibrated against a primary standard measured at Scripps (SIO 1986 calibration scale). Duplicated F-11 analyses of surface water samples give relative errors of $\pm 3\%$. The high detection limit ($0.05 \text{ pmol kg}^{-1}$) of the method on board is due to high blank levels associated with a refrigerator freon leak (F-12 data were lost because of this contamination).

A "Pegasus" current profiler of the University of Hamburg was dropped twice in the channel between Roti Island and Ashmore reef. To locate the instrument, three bottom transponders were fixed by GPS, which was working a few hours per day. Two exploratory subsurface current meter moorings were launched for one year: one in the strait between Roti and the Australian continental shelf, and one off the strait between Savu and Roti, outside the territorial waters (MOLCARD *et al.*, accepted).

3. WATER MASS CHARACTERISTICS

(A) Section Australia-Bali

Upper layer. In the surface layer, the isotherms 25 and 26°C (Fig. 3a) and the isopycnals 22.5 and 23 (Fig. 3e) present a general bowl shape corresponding to opposite relative baroclinic flows on each sides of the section, with a steeper slope on the Indonesian side consistent with a westward baroclinic flow. A bump in both isolines appears around Stas 6 and 10, possibly representing an eddy field. In the thermocline itself, which is sharp at those latitudes (24°C at 110 m–12°C at 320 m), the isolines are nearly flat from the Australian shelf up to 11°30S, then they slope upwards towards Indonesia. The 20°C isotherm, embedded in the thermocline, rises from 170 m in the south to 60 m near Bali, with two ridges at 140 m at Stas 6 and 10 (Fig. 3a). The F-11 and the oxygen isolines present the same structure with a low F-11 content up to 100–150 m near Bali (Fig. 3c and d). The upwelling near Bali (Sta. 19) reflects the effect of the easterly winds (Fig. 4) during that season which generate a strong westward surface current (Fig. 5), the Java current, which reverses with the monsoons (WYRTKI, 1961; ROCHFORD, 1969; QUADFASSEL and CRESSWELL, 1992); the coldest sea surface water, 23.66°C, is found off Bali (Fig. 3a). Mixed layer depths (defined as the depth within which temperatures do not differ by more than 1°C from the surface value) vary from 90 m to zero near the Indonesian coast despite strong winds there, with a mean depth of approximately 30 m.

A wedge of particularly low salinity surface layer less than 34.00 psu is encountered north of Sta. 7 (33.74 psu at Sta. 12) (Fig. 3b), while the historical mean values are between 34.00 psu and 34.50 psu (WYRTKI, 1961). The low salinities result both from the influx through the Indonesian archipelago of low salinity water from the Pacific and from local excess of precipitation over evaporation which characterizes the eastern quadrant of the Indian Ocean under the ITCZ. The particularly low salinity values could be related to the "La Nina" situation during that year (i.e. stronger trade winds over the equatorial Pacific ocean bringing more warm water towards Indonesia, increasing the atmospheric convective activity over the "maritime continent", and bringing more precipitations = opposite to the El Niño situation during which the precipitations decrease over that region). The cruise took place at the end of a "La Nina" event (PHILANDER, 1990). A relatively high salinity surface layer is found near the Australian continental shelf with more than 34.6 psu at Stas 2 and 3, where evaporation exceeds precipitation. Outside the upwelling region, in

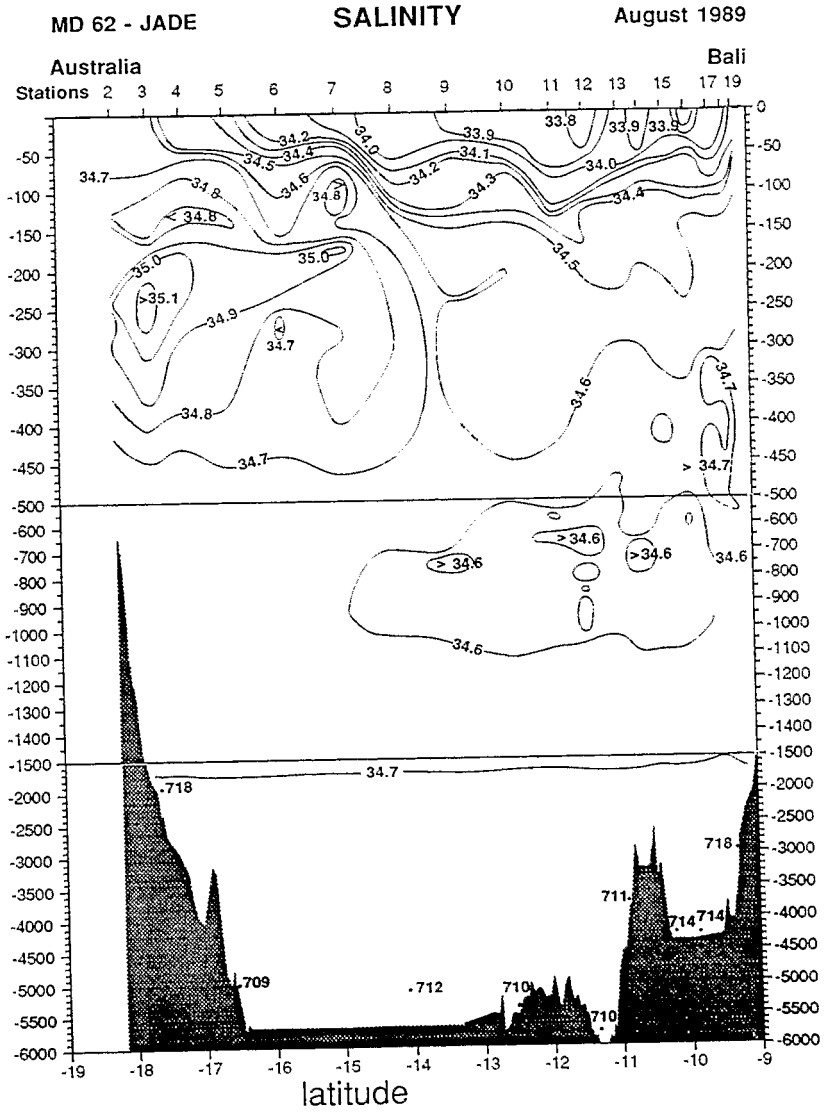


Fig. 3. (b).

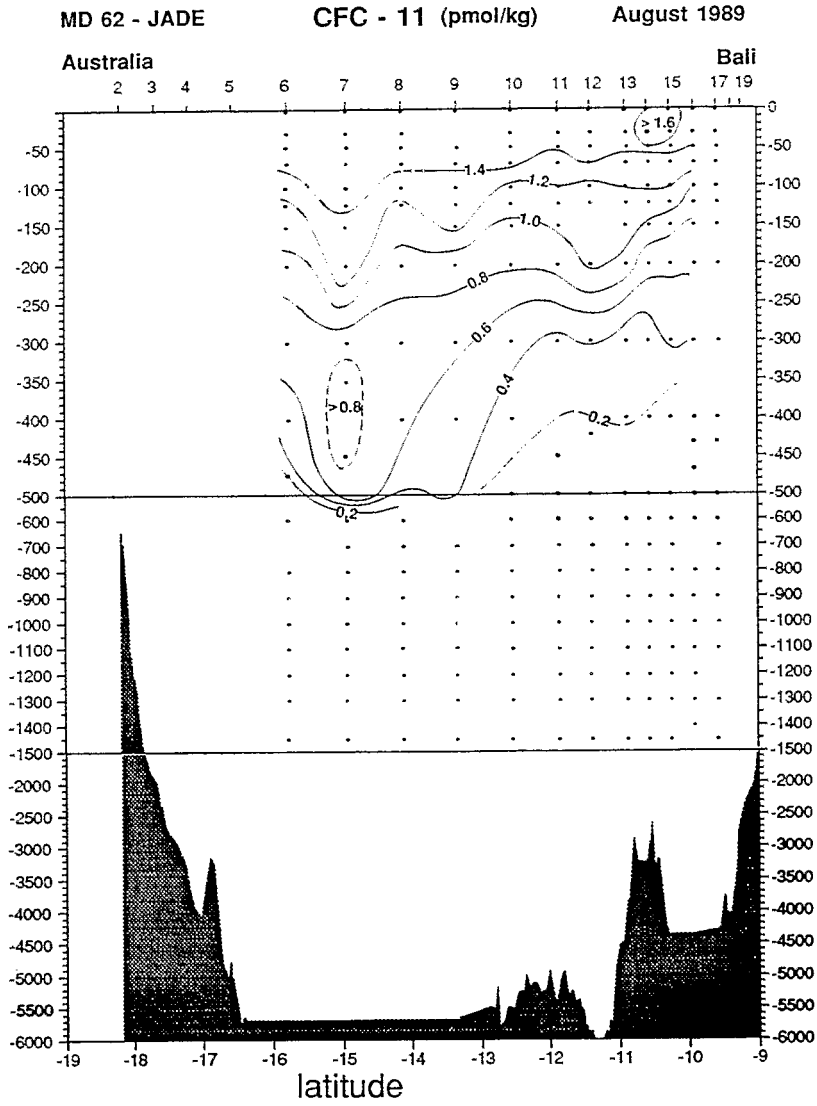
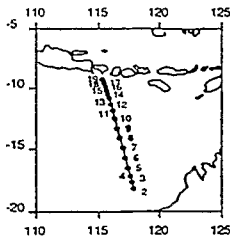


Fig. 3. (d).



JADE - MD 62 August 1989

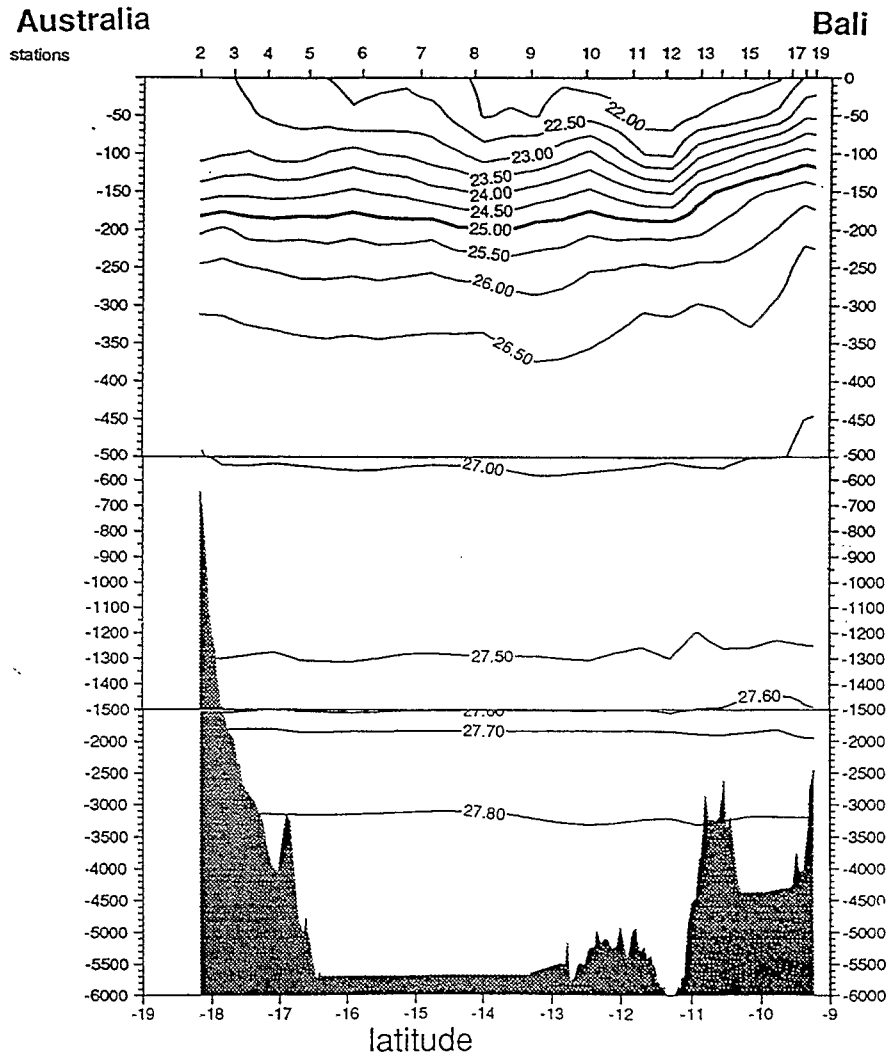


Fig. 3. (e).

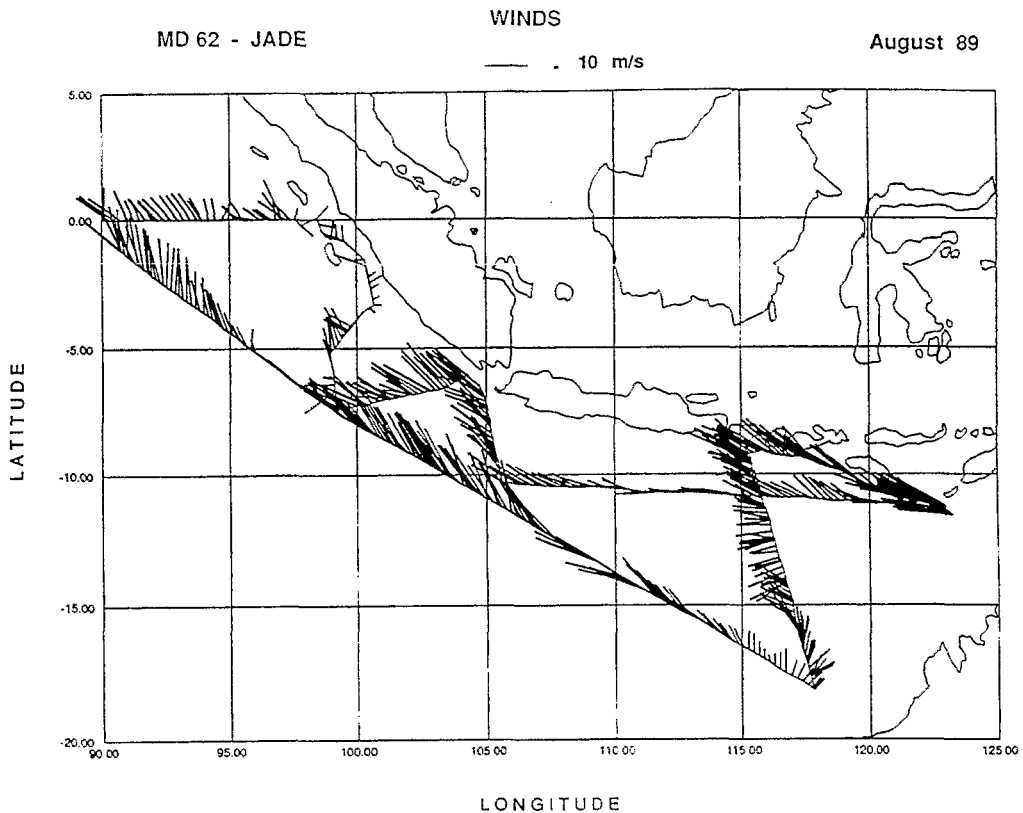


Fig. 4. Winds during the cruise in m s^{-1} .

the thermocline, the oxygen and F-11 contents present also similar features with deepening of the isolines at Stas 7 and 12. In the near-surface layers, 26–20°C, the θ - S curves for Stas 9–18 of the Australia–Bali section (Fig. 6a and c) lie generally within the limits defined by the outflows from the Savu and Timor seas, though with generally slightly higher salinities than the mixtures observed in the sections off the channels (Fig. 7a and c); there are also few bulbs of lower salinity than off the channels which could be due to the influence of water coming from the Java sea through Lombok strait.

Intermediate waters. The southern part of the section is close to the eastern end of WARREN's (1981a) section on 18°S, and the same sequence of water masses is observed here. Following his preferred nomenclature, the salinity maximum between 150 and 450 m (max 35.18 psu at Sta. 3, $\sigma_\theta = 26.06 \text{ mg cm}^{-3}$, Figs 6a and 3b) is identified as "Subtropical Water", formed by the excess of evaporation over precipitation in latitudes 25°S–35°S. The northern limit of the influence of this Subtropical Water is characterized by a sharp hydrological front between Stas 8 and 9, around 13°30S (this limit is given at 15°S along 110°E in ROCHFORD, 1969). The extension of this water mass between the Australian continental shelf and the 13°30S front is not regular: it is separated in two cores centered at

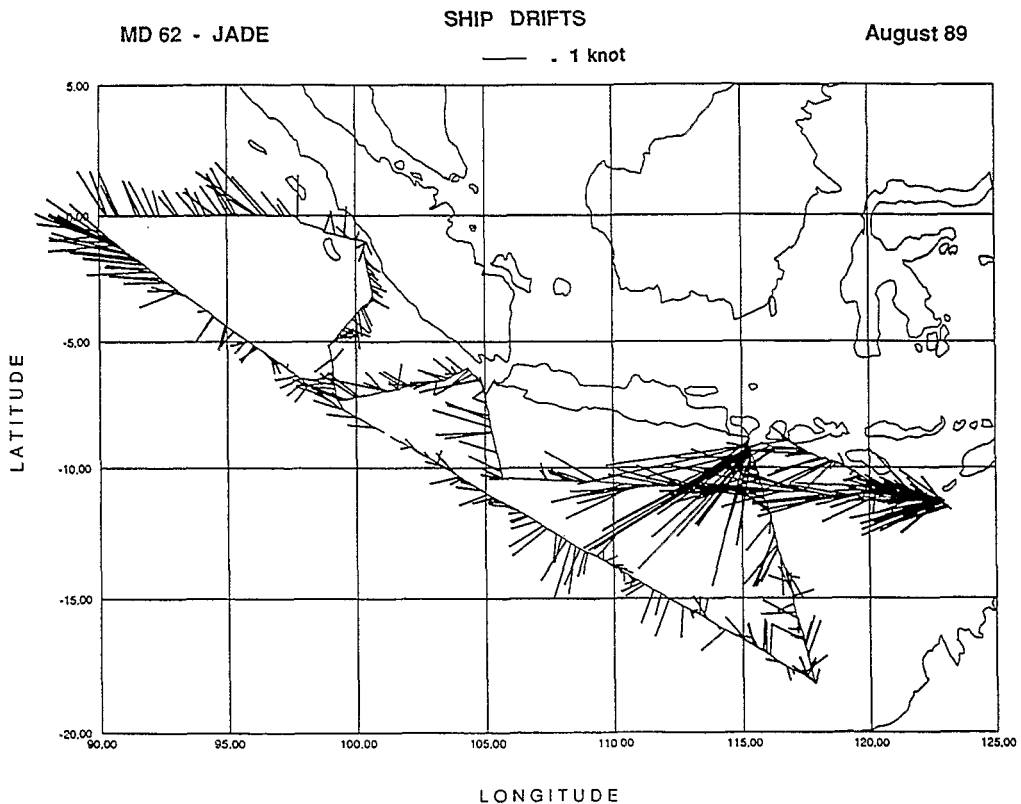
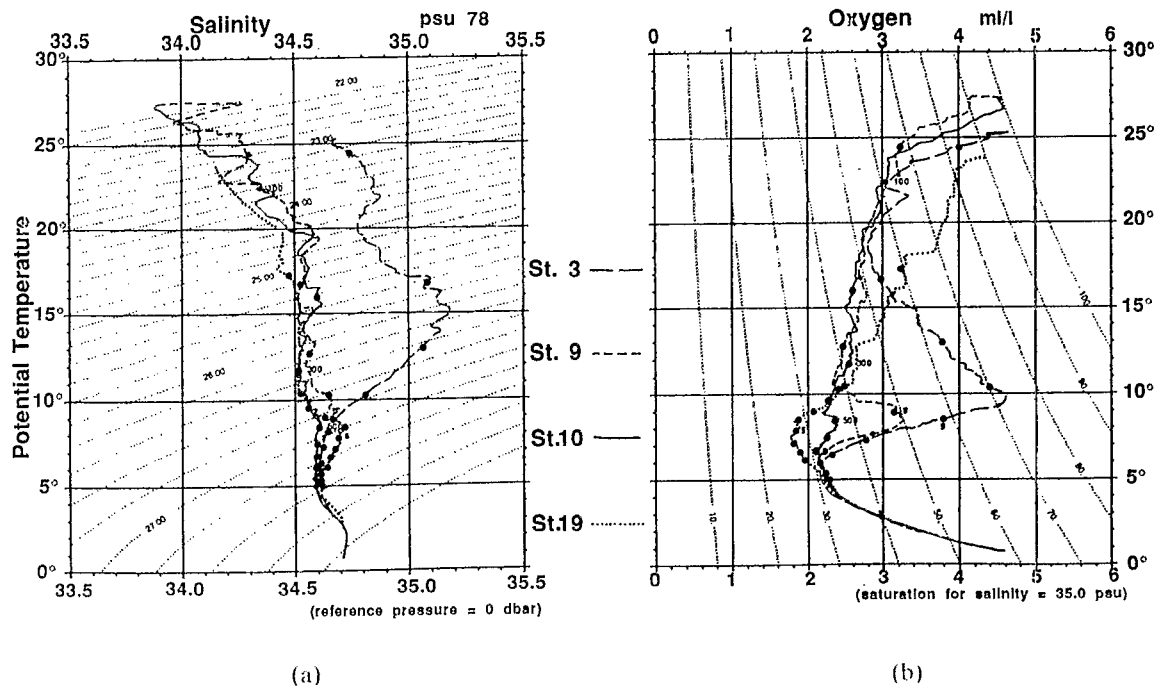


Fig. 5. Ship drifts during the cruise in knots.

Stas 3 and 7. Close to the continental shelf and at Sta. 6, appears some mixing with the lower salinity Indonesian water. Embedded in the high salinity layer (Subtropical Water), there is an oxygen minimum layer, centered around 200–350 m, with values $< 2.75 \text{ ml l}^{-1}$ (Figs 6b and 3c). In contrast, the F-11 values decrease steadily with depth through the oxygen minimum (F-11 > 0.6 , pmol kg^{-1} , Fig. 3d). This corroborates the conclusion that the oxygen minimum results mostly from *in situ* oxygen consumption (WARREN, 1981b). Further north along the section, this oxygen minimum is modified through mixing with the low oxygen content water coming from the Indonesian archipelago. North of the front, the salinities are much lower than in the south and close to the values found off the Indonesian straits at those depths (Indonesian waters); it is the main pathway of the throughflow waters.

Deeper, an oxygen maximum between 350 m and 600 m (max. 4.61 ml l^{-1} , on $\sigma_\theta = 26.80 \text{ mg cm}^{-3}$, 440 m, at Sta. 3, Figs 6b and 3c), is the continuation of the maximum formed by relatively deep vertical convection in the southern Indian Ocean, in latitudes 40–50°S, north of the subtropical convergence (see the discussion in WARREN, 1981a), named also Mode Water (MCCARTNEY, 1977). It is convenient to refer to this by the old name of "Indian Ocean Central water" (SVERDRUP *et al.*, 1942). Here the oxygen maximum is



(a)

(b)

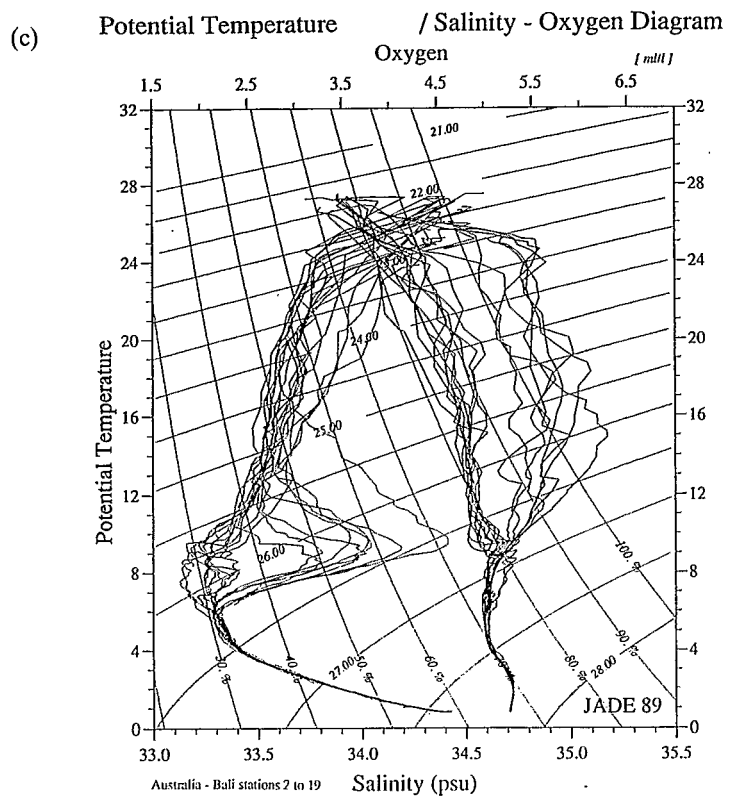
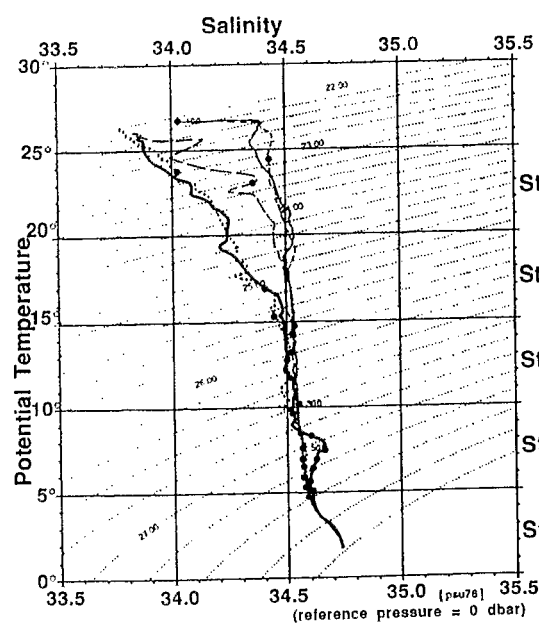
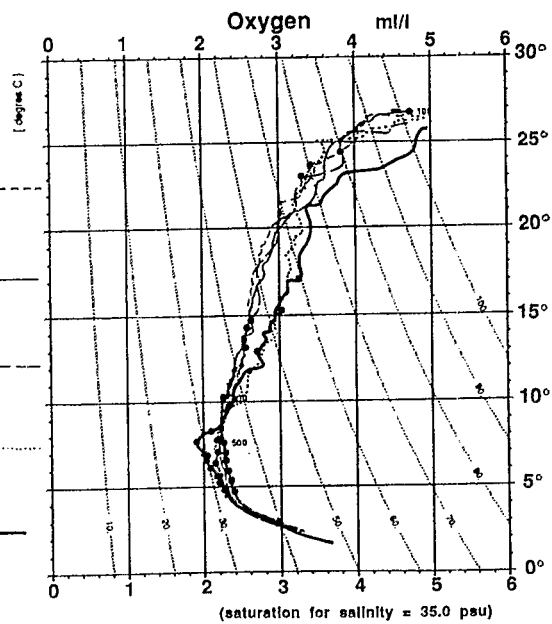


Fig. 6. (a) θ - S diagrams for Stas 3, 9, 10 and 19 between the Australian continental shelf and Bali; (b) θ - O_2 diagrams for the same stations (points on the curve each 100 dbar to 1000 dbar); (c) θ - S and θ - O_2 diagrams for all the Stas 2-19.



(a)



(b)

(c) Potential Temperature / Salinity - Oxygen Diagram

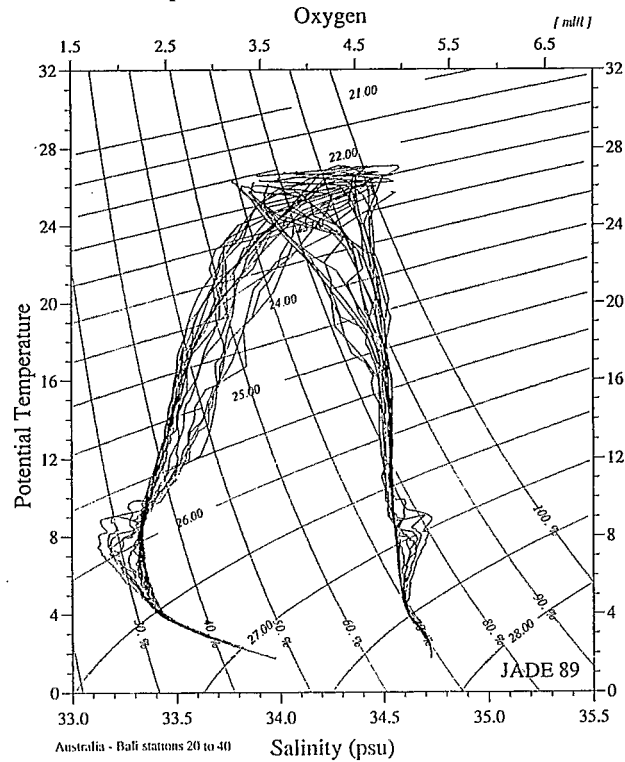


Fig. 7. (a) θ - S diagrams for Stas 22, 26, 29, 34 and 37 (points on the curve each 100 db to 1000 db); (b) θ - O_2 diagrams for the same stations; (c) θ - S and θ - O_2 diagrams for all the Stas 20-40.

separated in two cores by the water found at Sta. 6 which is a mixture with Indonesian water of lower oxygen content (coming from the Banda sea), also present along the shelf at Sta. 2. The northern oxygen maximum core is correlated with higher values in F-11 content ($>0.8 \text{ pmol kg}^{-1}$ between 14 and 16°S, Fig. 3d) which means that this water mass is "younger", i.e. has been ventilated more recently or is less mixed, than the water north and south of it. Note that there are no F-11 data for the southern core where the highest oxygen maximum is found at Sta. 3. The cores of high salinity and high oxygen content, although not at the same depths, are found at the same stations (Stas 3 and 7) but their extension to the north is slightly different. The high salinity core is bounded by the sharp front around 13°30 S. North of 13°30 S, in the layer $25.2 \text{ mg cm}^{-3} < \sigma_\theta < 26.4 \text{ mg cm}^{-3}$, the water mass characteristics are close to those of the waters near the channels (Figs 6c and 7c). Below, the influence of the lower part of the oxygen maximum of the Central Water can be traced further north, between 500 and 600 dbar, up to Sta 13 (10°52 S). The relative oxygen maximum is enhanced by the variation of oxygen solubility with temperature. The usual minimum potential vorticity signature of the Mode water has been eroded by mixing along its path from the formation region and cannot be found here.

Between Sta. 14 and the Indonesian coast, in the layer $300\text{--}800 \text{ m}$ ($26.70 \text{ mg cm}^{-3} < \sigma_\theta < 27.25 \text{ mg cm}^{-3}$), appears a different water mass characterized by higher salinity ($S > 34.7 \text{ psu}$) and lower oxygen concentration ($O_2 < 2.0 \text{ ml l}^{-1}$), particularly well marked at Stas 17 and 19. This water mass cannot come from the Indonesian seas where no such low oxygen nor high salinity values are found (BROECKER *et al.*, 1986; VAN AKEN *et al.*, 1988). Its characteristics can be related to the high salinity, low oxygen intermediate waters of the Arabian sea (Northern Indian Ocean Water or NIW), diluted by spreading through the equatorial band (see the charts of salinity and oxygen, Oceanographic Atlas IIOE, WYRTKI, 1971, pp. 283–285). The spatial distributions of salinity and oxygen content in the upper part of this layer, for example on $\sigma_\theta = 26.80 \text{ mg cm}^{-3}$, using data from the stations carried out off Sumatra, show the evolution of the salinity maximum and oxygen minimum from the equator to the channels (Fig. 8a and b). The NIW seems trapped along the Sumatra–Mentawai–Java coasts and Java ridge in several cores. The region north of the hydrological front is a region of intense mixing between the water masses coming from the Indian Ocean (the Subtropical Water and the Central Water coming from the south and the Northern Indian Ocean Water coming from the north) and the waters coming from the Indonesian seas (the Banda Sea Water, water mass formed by mixing of North Pacific Subtropical Water and Pacific Intermediate Water and some water from the shallow and low salinity Java sea (WYRTKI, 1961). The corresponding oxygen content values are slightly lower than off the sills which implies mixing with NIW. The arrows in Fig. 8a and b give a possible interpretation of the circulation from these property distributions describing the intense mixing. The spatial distribution of F-11 at 400 m ($26.6 < \sigma_\theta < 26.9$), despite the high blanks level, shows the same features which reflect in particular that the Indian Ocean Central Water is the youngest water at those depths (Fig. 8c). The intense mixing region north of the hydrological front and south of the NIW core is the throughflow main region which represents the eastern part of the so-called "Equatorial Frontal Zone" (EFZ) of the Indian Ocean (WYRTKI, 1961; ROCHFORD, 1969). This EFZ is taken as the hydrological limit between the northern and the southern Indian Ocean. Contrary to the Pacific and Atlantic oceans, this hydrological limit is far south of the actual Equator in the Indian Ocean. The position of the EFZ in the Indian Ocean seems to be related both to

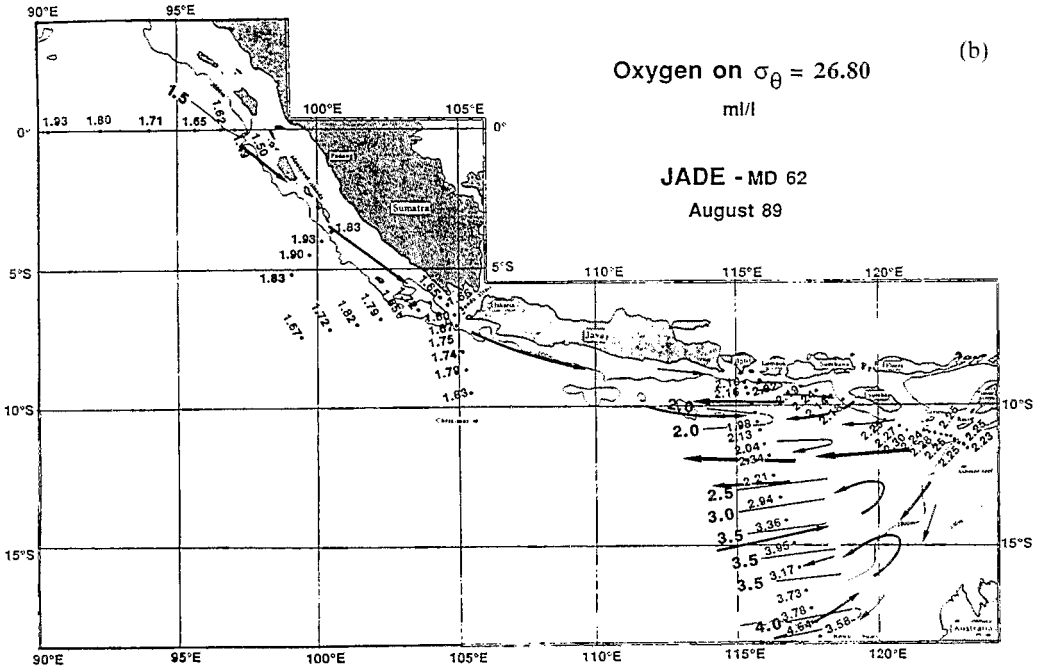
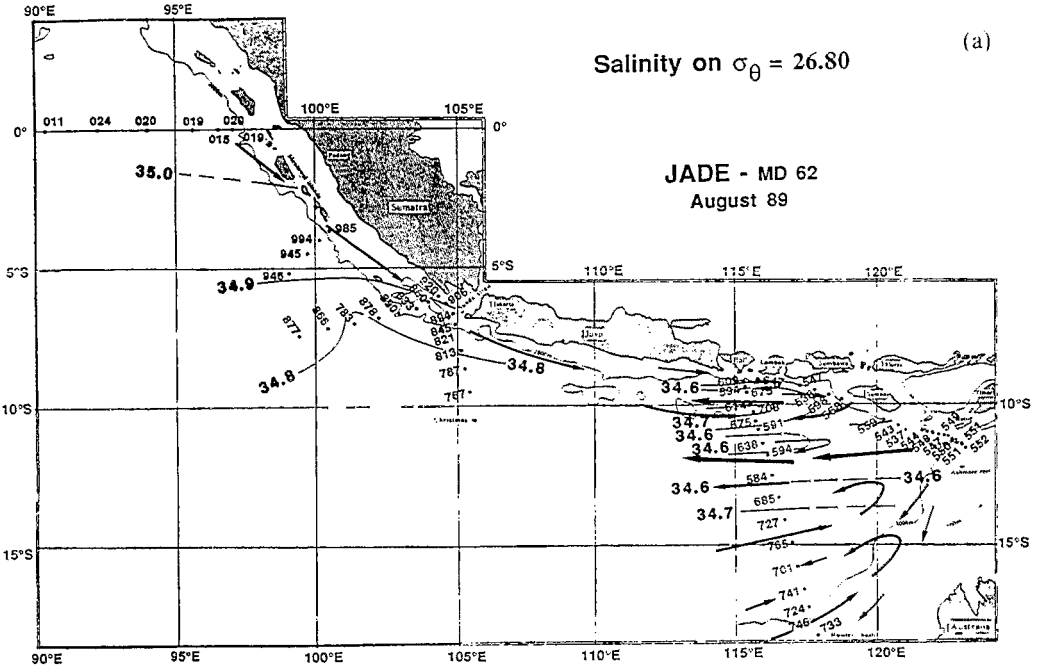
the seasonal southern limit of the ITCZ (Intertropical Convergence Zone) and to the latitudes at which the throughflow emerges into the Indian Ocean (9–13°S).

Between 750 m ($\sigma_\theta = 27.2 \text{ mg cm}^{-3}$) and 1000 m ($\sigma_\theta = 27.4 \text{ mg cm}^{-3}$) there is a weak salinity minimum (34.58–34.61 psu) (Fig. 6a). This salinity minimum is associated with an oxygen minimum just above ($2.1 \text{ ml l}^{-1} < \text{O}_2 < 2.2 \text{ ml l}^{-1}$, Fig. 6b, Stas 3–10). Near the Australian continental shelf it is a faint signature of Antarctic Intermediate Water influence ($S = 34.61 \text{ psu}$, Stas 4 and 5). North of Sta. 8, mixing with the contribution coming from the Indonesian archipelago (called “Banda Intermediate Water” by ROCHFORD, 1966) leads to lower minimum salinities ($S = 34.58 \text{ psu}$, Stas 13–15). The spatial distribution of salinity (Fig. 9a) and oxygen content (Fig. 9b) on $\sigma_\theta = 27.2 \text{ mg cm}^{-3}$ shows a pattern similar to the spatial distribution on $\sigma_\theta = 26.8 \text{ mg cm}^{-3}$ with the influence of the NIW in the north (high salinity and low oxygen). The same features persist with an attenuated form in the salinity and oxygen distributions below 1000 m to about 2000 m ($27.4 \text{ mg cm}^{-3} < \sigma_\theta < 27.70 \text{ mg cm}^{-3}$); at Sta. 19, nearest to Bali, slightly higher salinity and lower oxygen demonstrate NIW influence down to 1700 m ($\sigma_\theta = 27.65 \text{ gm cm}^{-3}$) (Figs 6a and 3c).

Deep waters. The salinity maximum of the “Deep water” coming from the southern Indian Ocean is found around 2400 db ($\sigma_\theta = 27.76 \text{ mg cm}^{-3}$, Fig. 6a) with values between 34.723 and 34.728 psu. Deeper, the salinity decreases towards the bottom and the oxygen content continues to increase up to 4.6 ml l^{-1} which marks the influence of the younger and colder “Circumpolar Deep Water”. The Western Australian basin is open at depth to the Antarctic influence by the way of the Perth basin and the Circumpolar Deep Water can flow northwards as a deep western boundary current on the eastern flank of the 90°E ridge (WARREN, 1981a). The extreme characteristics on this section are found at Sta. 12 in the Java Trench near 11°30S at 5800 db ($S = 34.710 \text{ psu}$, $\theta = 0.784^\circ\text{C}$, $\text{O}_2 = 4.62 \text{ ml l}^{-1}$, $\sigma_\theta = 27.826 \text{ mg cm}^{-3}$). The Lombok basin lies between the Java ridge and the Sunda arc islands; its bottom water characteristics are $S = 34.714 \text{ psu}$ and $\theta = 1.015^\circ\text{C}$ (deepest observation at 4279 m) and correspond to the characteristics found in the open northwestern Australian basin at around 3650 m. It means that the Lombok basin is closed by the Java ridge at depths deeper than 3650 m.

(B) Section Bali–Timor trench

Surface mixed layers on this section (Fig. 2) are generally deeper (10–100 m, mean = 50 m), cooler and slightly more saline than those at Stas 9–18 in the outflow region of the Australia–Bali section. This is presumably the result of increased wind stress (Fig. 4). Above 15°C, the water mass characteristics vary from one channel to another, as can be seen in the θ – S diagrams of Fig. 7a. They can be divided into three groups: (1) an almost constant gradient from around $\theta = 26^\circ\text{C}$, $S = 33.8 \text{ psu}$ to $\theta = 16^\circ\text{C}$, $S = 34.5 \text{ psu}$ (Stas 22, 23, 25, 26 and 27); (2) a relatively steady salinity exceeding 34.35 psu from 25°C downwards, below a sharp halocline (Stas 33–40); and (3) a more variable intermediate group occupying the space between those two in the θ – S diagram (all the remaining stations, example Sta. 29 on Fig. 7a). The first group, with the lowest salinities, are interpreted as unmixed water coming directly from the Savu sea, on both sides of Sumba. The higher salinities of the second group (under the sharp halocline) representing the



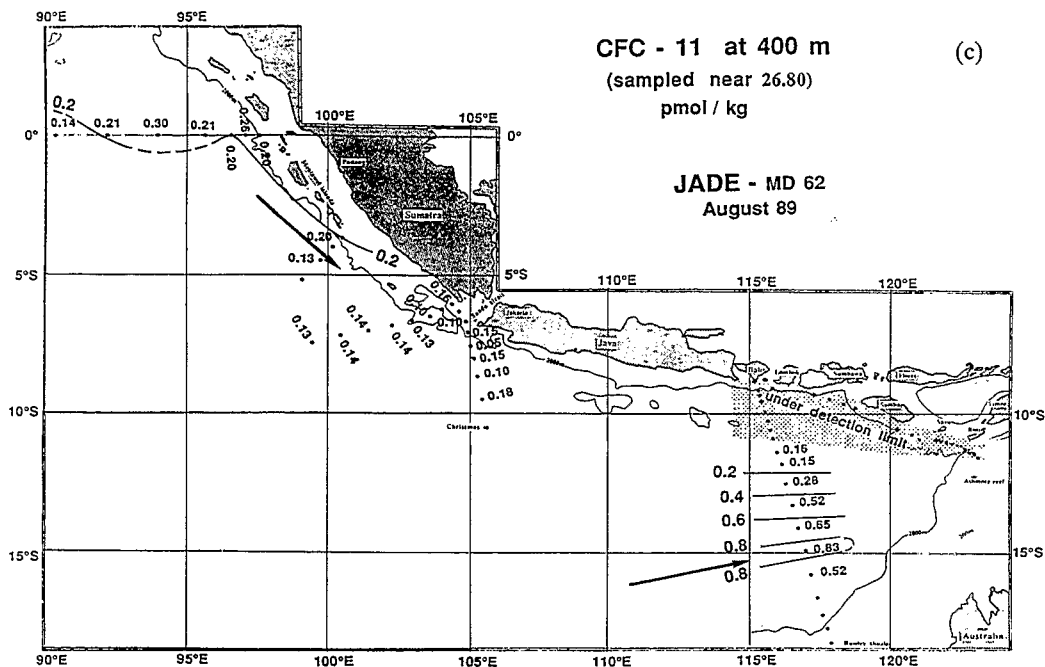


Fig. 8. (a) Spatial distribution of S , on $\sigma_\theta = 26.80$; (b) Spatial distribution of O_2 , on $\sigma_\theta = 26.80$; (c) spatial distribution of CFC-11 at 400 m (depth of the samples, see Fig. 3d).

outflow from the Timor sea, are a consequence of more exposure to drying southeasterly winds (WYRTKI, 1961) and being open to exchange with warm higher-salinity surface water of the northwest Australian continental shelf (WYRTKI, 1971). The third group are interpreted as a mixture of the first two, with probably some contribution from the higher-salinity near-surface waters of the Indian Ocean present in the Australia-Bali section south of Sta. 8. A notable feature appears in the middle of each channel: there is a core of low salinity ($S < 33.90$ psu) high oxygen ($O_2 > 4.75$ ml l^{-1}) high temperature ($> 26^\circ C$) water between 0 and 50 m indicating relatively fresh surface water coming from the Indonesian seas where the precipitations are high due to the active atmospheric convection (Fig. 10a and b). These characteristics suggest a faster flow coming from the east in the middle of the channels (Fig. 5) and active mixing in the surface layers on each side.

Below the thermocline (Fig. 10c), in the western part of the section (Stas 19-25), off Lombok and Sumba straits, the salinity maximum-oxygen minimum layer between 380 m and 800 m (Figs 7a and b; 10a and b) ($26.8 < \sigma_\theta < 27.3$ mg cm^{-3}), marks the influence of the NIW observed in the northern part of the Australia-Bali section. Our data set is limited to the Indian Ocean side of the channels, so we cannot say how far this influence extends towards the Savu sea through Sumba strait. In the other channels southeast of Sumba, water mass characteristics suggest westward flow in that depth range. In Timor channel, below the halocline, the vertical salinity gradient is very small; the salinity varies

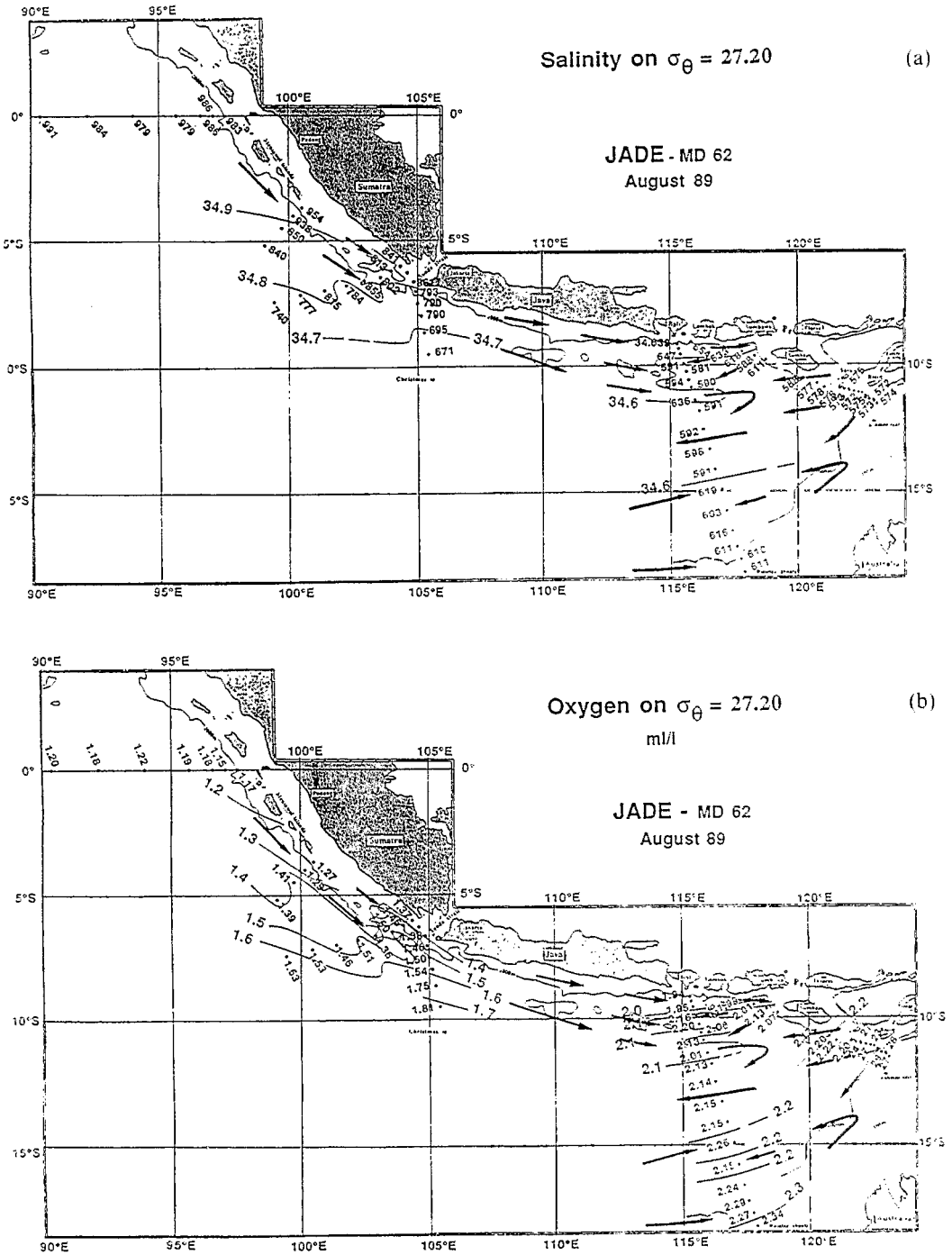


Fig. 9. (a) Spatial distribution of S , on $\sigma_{\theta} = 27.20$; (b) spatial distribution of O_2 , on $\sigma_{\theta} = 27.20$.

from 34.538 psu at 200 m to 34.599 psu at 1100 m (Sta. 34) corresponding to the values found inside the Indonesian seas (Banda sea water, WYRTKI, 1961; BROECKER *et al.*, 1986; VAN AKEN *et al.*, 1988). It follows that the Subtropical water from the Indian Ocean was not entering the Timor sea nor the Savu sea. Deeper than 1400 m, there is an increase of salinity and oxygen content corresponding to the influence of the Deep water coming from the Indian Ocean (Figs 7a and b; 10a and b). On the Timor trench sill which lies around 1900 m, the upper part of the Deep water is present (Stas 34 and 39) below 1400 m ($\sigma_\theta = 27.5 \text{ mg cm}^{-3}$) (Fig. 7a and b). These values of salinity ($S > 34.7$ psu) and oxygen content ($\text{O}_2 > 3 \text{ ml l}^{-1}$) are higher than the ones found in the Banda sea. So the upper part of the Deep Water can enter the Timor basin but cannot reach the eastern seas directly without upwelling and strong mixing. It is also possible that this water returns back to the Indian Ocean through the same strait.

4. CURRENTS AND TRANSPORTS

(A) Surface drifts

The cruise took place during the peak of the southeast monsoon. Over most of the surveyed region, the winds were southeasterly except south of 15°S where they were southwesterly (Fig. 4). Wind speeds varied between 7 and 13 m s^{-1} . As expected under the southeast monsoon, the general surface drifts are towards the west-southwest in the Bali-Timor section and in the northern part of the Australia-Bali section, with speeds between one and two knots (Fig. 5). The strongest surface drift encountered was 4.5 knots southwestward south of Bali, at the mouth of the Lombok strait, which shows up also in the historical ship drifts (RICHARDSON and MCKEE, 1989). South of 16°S , the surface drifts are weaker and much more variable, with a tendency, like the winds, towards the east. Surface drifts observed at stations in the Bali-Timor section (Fig. 5) indicate relatively strong outflow from the channels on both sides of Sumba and from the Timor sea, and weaker evidence of outflow from the channel between Savu and Roti, consistent with the θ - S characteristics mentioned above. Another feature to be noted is the convergence of the surface drifts between the two sections along Sumatra, north and south of 6°S , despite the same direction of the winds.

The Ekman layer transport through the section Australia-Bali calculated with the observed winds amounts to -1.4 Sv ($10^6 \text{ m}^3 \text{ s}^{-1}$) towards the southwest (with $c_D = 1.5 \times 10^{-3}$). Through the Bali-Timor section, with a greater wind stress more aligned with the section, the Ekman transport towards southwest is -5.3 Sv . If we use the HELLERMAN and ROSENSTEIN (1983) monthly mean wind stress, we get -1.5 Sv for the Australia-Bali section and -1.9 Sv for the Bali-Timor section. The latter value seems more reasonable for the Bali-Timor section. The -5.3 Sv is large, and probably the transport had not settled down into equilibrium with the increased wind stress.

(B) Pegasus current profiles

We had the opportunity to make two Pegasus current profiles (collaboration of K. Schulze and D. R. Quadfasel, University of Hamburg) on the Timor trench sill, close to Stas 34-39 (Fig. 11). The profiles indicate a flow towards the Indian Ocean down to 1200 m. There is a maximum towards the southwest at 200 m which reaches 50 cm s^{-1} ; between

(a)

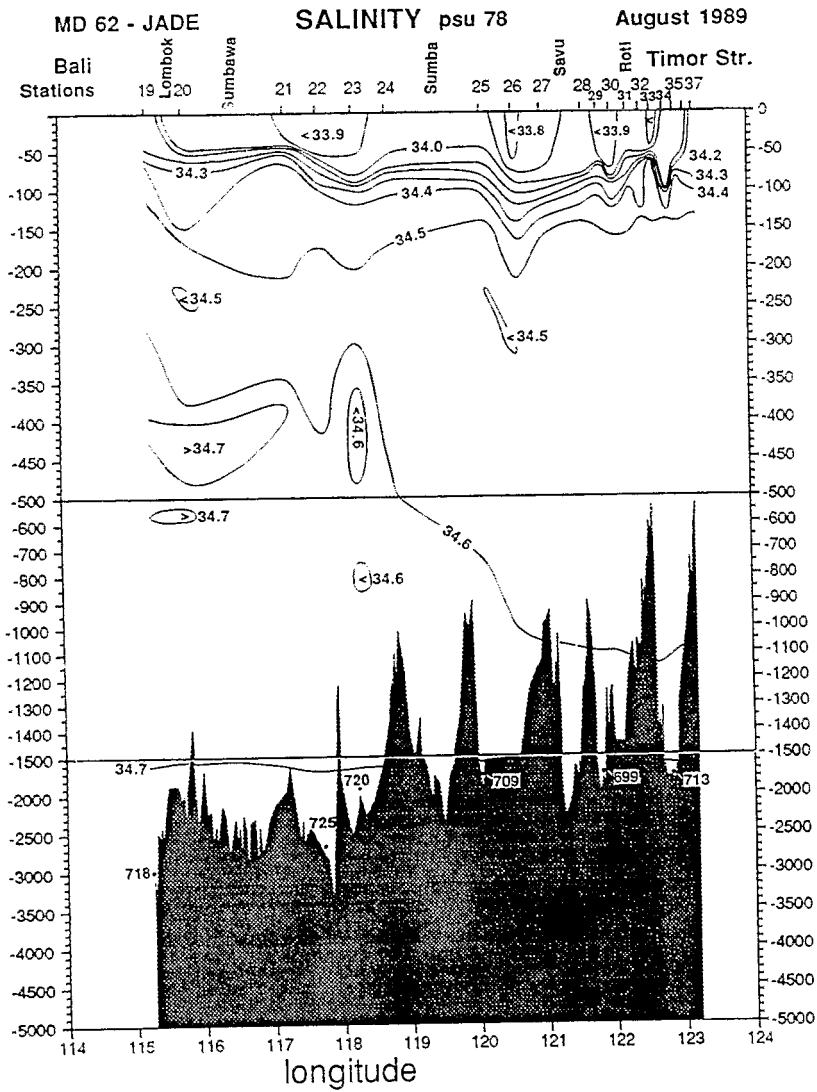


Fig. 10. (a).

(b)

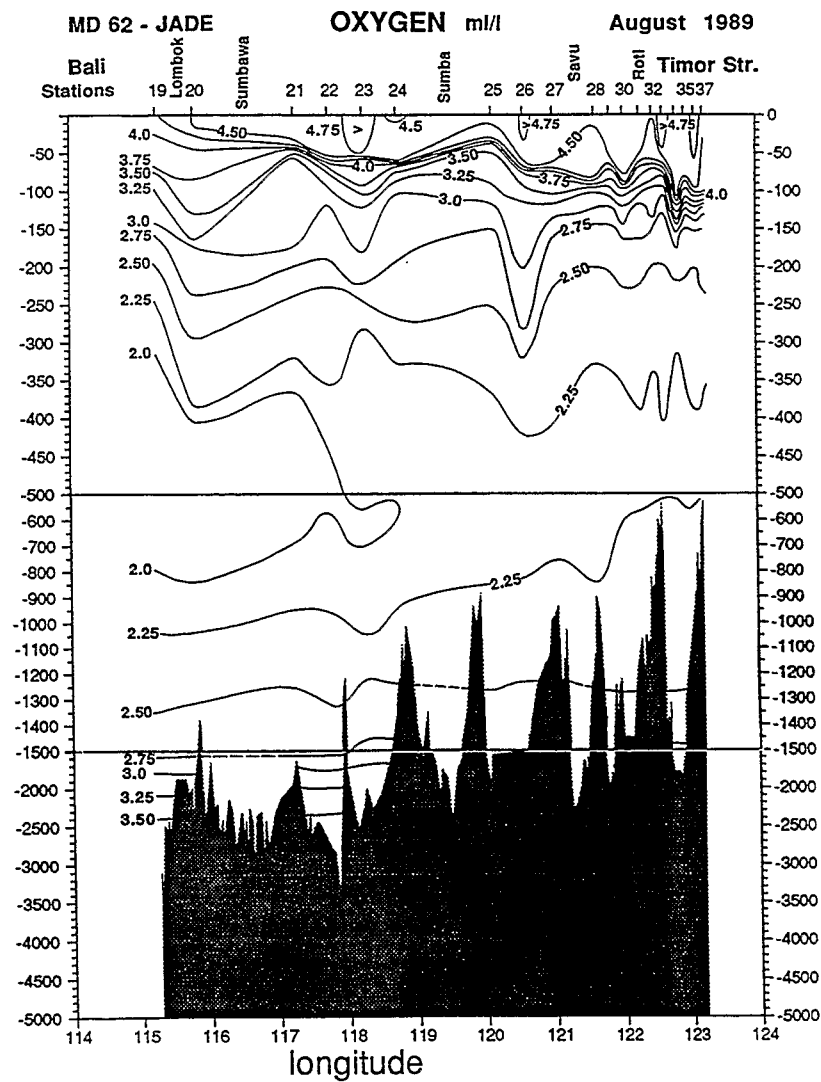


Fig. 10. (b).

(c)

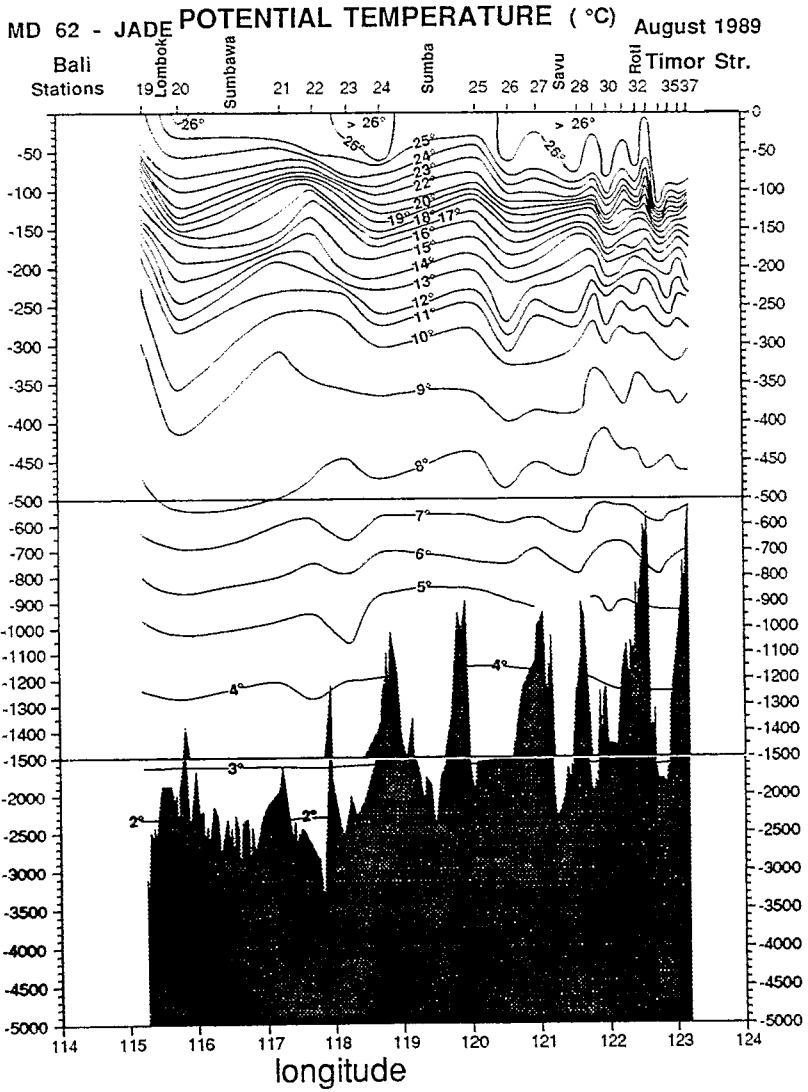


Fig. 10. (c).

(d)

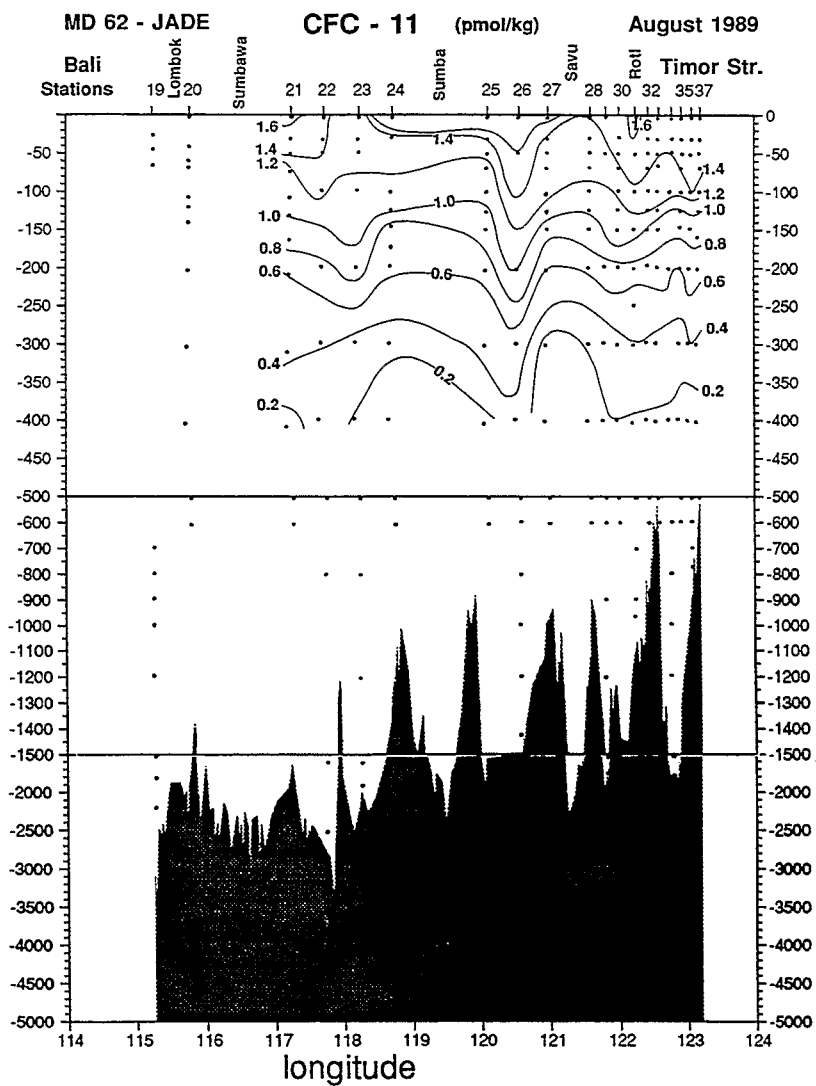


Fig. 10. (a) Salinity section Bali-Timor trench (lines at 500 db and 1500 db note a change of scale); (b) oxygen section Bali-Timor trench; (c) temperature section Bali-Timor trench; (d) CFC-11 section Bali-Timor trench (dots correspond to the samples depths).

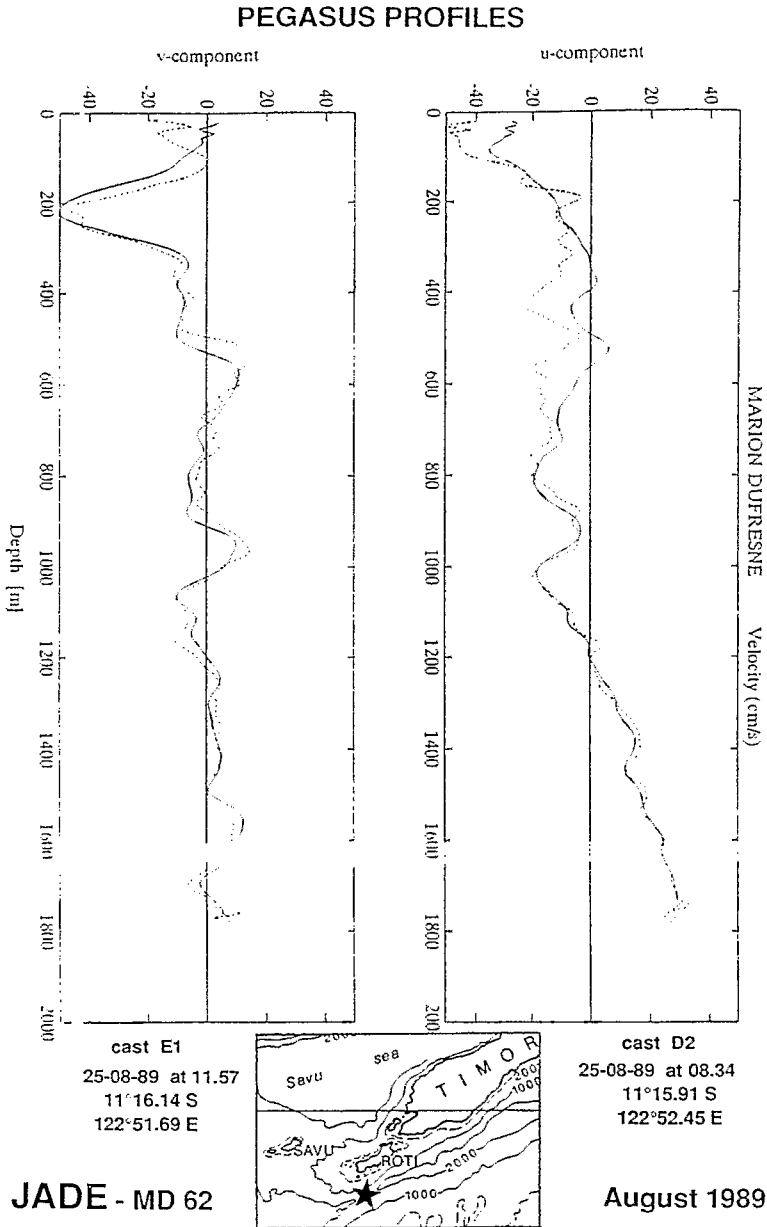


Fig. 11. Two current profiles on the sill of Timor trench obtained with the Pegasus profiler (University of Hamburg, K. Schulze).

400 and 1000 m the current is weaker (less than 10 cm s^{-1}). The current reverses towards the east below 1200 m down to the bottom, where currents reach 30 cm s^{-1} . This important but pin-point observation, revealing a transport towards the east at depth, is in agreement with the water mass characteristics presented above (Fig. 7a and b). The two profiles (up and down) were done 3 h 20 min apart and are very coherent, through differences can reach 15 cm s^{-1} possibly due to tidal variability.

(C) Moorings

On the mooring launched on the Timor sill, between the Australian continental shelf and Roti island, the currents were measured between 100 and 1000 m (MOLCARD *et al.*, accepted). The mean current profile over one week after the launching, shows, as did the Pegasus, a maximum at 200 m of 40 cm s^{-1} then a decrease towards the bottom. The geostrophic current profile computed from averaged (because of tidal variability) stations north and south of the sill shows a similar maximum at 200 m but only half the speed. The estimates of the transport through the channel from the direct current measurements between 100 and 1000 m, during the week following the launching, are between 9 and 5 Sv, respectively, if the current is considered the same across the channel or decreasing to zero at the channel boundaries. If we take the mean value of 7 Sv for the transport, it is about half of the westward geostrophic transport estimated in that layer on the section Australia-Bali.

(D) Geostrophic transports

Transports across the Australia-Bali section. In a first approach, geostrophic currents and transports were calculated using the deepest casts at each of the Stas 2-19 (Fig. 2) with different reference levels chosen between 800 db (mean depth of the oxygen minimum layer in the southern part of the section) and 2200 db (the deepest common level for most of the stations, and well below the sill depth of any of the channels connecting the Indonesian seas to the Indian Ocean), among which 1200 db (flow reversal observed in the Timor channel at that depth) and 1900 db (depth of the deepest sill (Timor channel), so the basin to the east of the section is closed at that level). For station pairs that did not reach the chosen reference level, zero velocity was assumed at their deepest common level. At the ends of the section we extrapolate to the 200 m isobath, taking the current calculated for the adjacent pairs of stations and assuming that the current tapers off linearly to zero at the slope.

The net (geostrophic + Ekman) transports integrated over the whole section for those different reference levels are very similar, particularly in the upper layers. Most of the westward transport is confined to the upper layers (between 23 and 26 Sv in the upper 500 db) as can be seen on the profile of the transport per unit depth relative to 2200 db (Fig. 12) which shows also that any reference level below 500 db would have given similar results. Because, compared to the previous indirect estimates, these transports are so large, we will try to estimate their uncertainties.

At five of the stations in the section, repeated casts were made to 2200 db or more. Those pairs of casts show appreciable variability in dynamic heights. The differences have a fairly simple structure in the vertical, but vary from one station pair to another. For the central part of the section, we can make up two versions of the geostrophic transport relative to

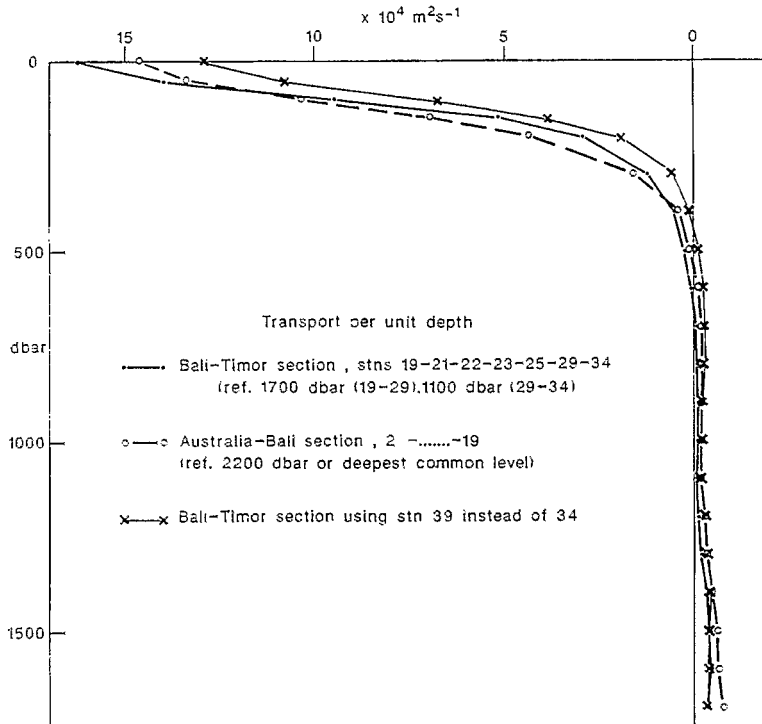


Fig. 12. Transports per unit depth for the section Bali-Timor (using either Sta. 34 or the repeat Sta. 39) and for the section Australia-Bali.

2200 db; one using the full-depth casts at Stas 5, 8, 10, 12 and 16 (Fig. 2), the other using the 2200 db casts. Separated by an average of only 4.2 h, there should be no real difference in their transports. However, the curves in Fig. 13 show substantial differences below 500 db. The net transports for this part-section, 0–2200 db, are 17.3 and 12.2 Sv westwards for the deep and 2200 db casts respectively, a difference of 5.1 Sv. One wonders whether the difference could be caused by some instrumental fault in the CTD making the deep casts somehow “bad”. The section made from the 2200 db casts has a zero crossing at 1200 db (relative to 2200 db), and eastward transport below that, consistent with the Pegasus current profile in the Timor strait, and the deep water properties. On the other hand the “deep cast” transport profile in Fig. 13 is reassuringly steady between 1900 and 3400 db, consistent with little or no transport deeper than the Timor channel sill (the shear in the transport profile below 3600 db is not surprising; Sta. 16 is in the Lombok basin, separated from the other deep stations in the North Australia basin by the Java ridge). So, it is difficult to understand how the deep casts could be “good” below 1900 db and “bad” above. We conclude that apparent differences in geostrophic transport are caused by real fluctuations in dynamic heights, probably related to semidiurnal tides. The “noise” in these transport estimates is not cumulative along the section, but will presumably still be present at the end stations, so that the uncertainty in transport for the whole section will not be less than the 5 Sv noted above for part of the section. Moreover, this must be a lower

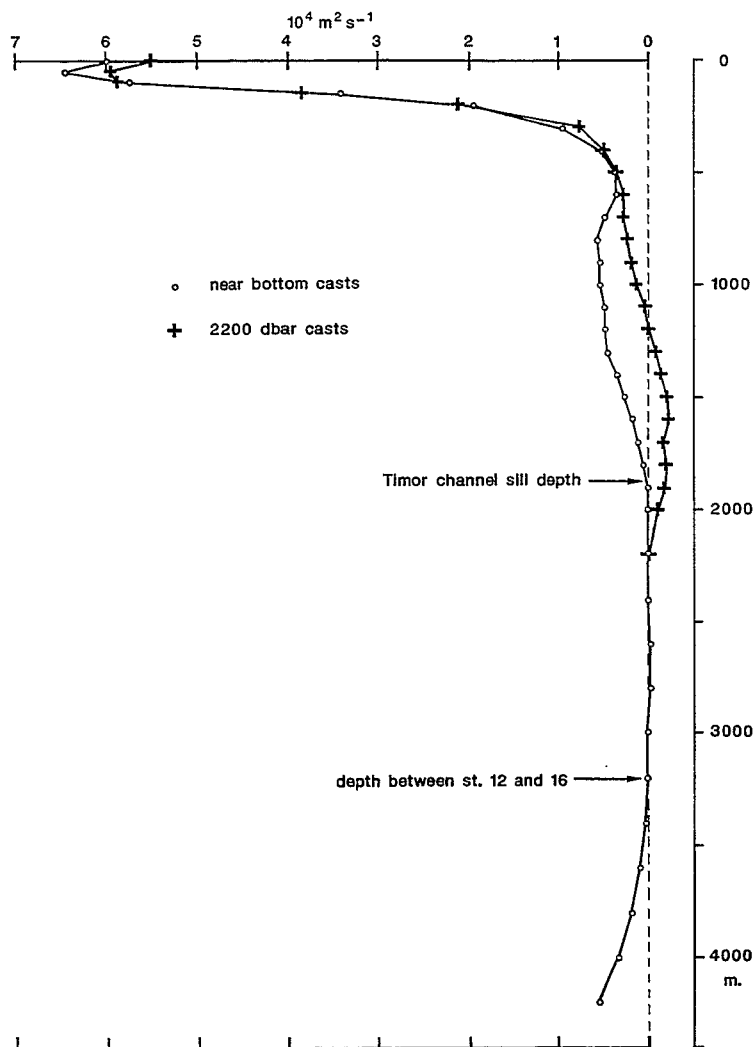


Fig. 13. Vertical distribution of transport per unit depth between deep stations (Stas 5, 8, 10, 12, 16) in Australia-Bali section, and between 2200 db casts done at the same stations.

limit, since much of the geostrophic variability of dynamic heights may have been missed with an average repeat interval of only 4.2 h.

Comparison of geostrophic surface currents with the corresponding mean components of observed ship drifts gives another estimate of their uncertainty (Fig. 14). The much greater variability of the geostrophic surface currents, if applied through a layer 100 m thick, with an average station spacing of 67 km, would correspond to an uncertainty in geostrophic transport for that layer of ± 2 Sv. The differences in transport, using the same stations but different choices of reference level, are not much greater than these expected uncertainties. The profiles in Fig. 13 lend support to a use of 1900 db or below, as a most

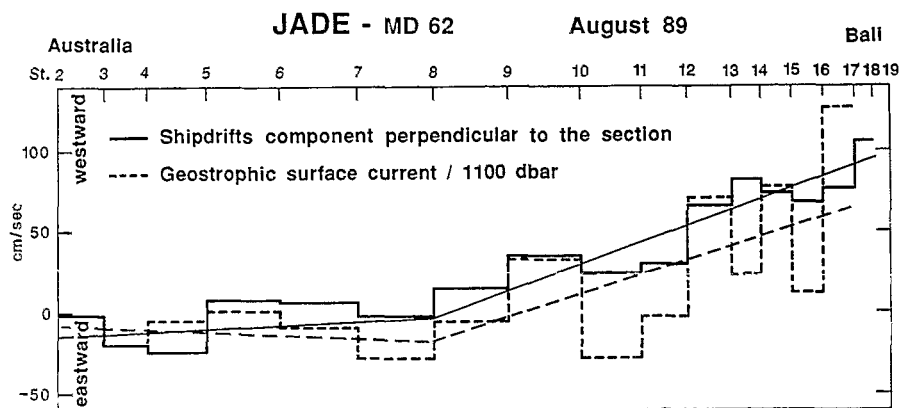


Fig. 14. Geostrophic surface currents and component of ship drifts along the section Australia-Bali in cm s^{-1} .

suitable reference level for Stas 5–16, and the weak shear observed between Stas 2–5 allows the use of same reference level, or the deepest common level, for the southern end of the section. Two problems arise, however, with the transports north of Sta. 16. Figure 15 shows that, relative to any deep reference level, at intermediate depths there is a strong reversal of geostrophic transport between Stas 16, 17 and 19 (Sta. 18 had to be cut short at 445 db in bad weather and is not used here; Sta. 19 was occupied 4 days later). That reversal of transport coincides with the salinity maximum of the NIW, shown on the right of Fig. 15. One might take the view that the sudden change in salinity at 300 db at Sta. 17 could indicate a suitable reference level, with low-salinity water above going westward and high-salinity water going eastward below. For Stas 16–17, however, that would imply an unrealistic transport below the 1900 db sill depth of 50 Sv eastward. A more moderate assumption would be to regard the profiles in Fig. 15 as evidence of a rotating lens of high salinity NIW, and to require a reference level at 300 db only for the mean velocity between Stas 16 and 19. Even that, however, would imply an excessive transport of about 20 Sv below 1900 db. It seems preferable to keep to the assumption of negligible transport below sill depth, and to admit the inconsistency with the salinity profile in the region of 300–400 db. This may not be too serious: current measurements in the Timor trench (MOLCARD *et al.*, accepted) showed appreciable variability with time-scales of a month or less, so the transport through this section is unlikely to have been steady. The second problem with Stas 16–19 is that their transport-per-unit-depth profile (Fig. 15) is not as steady below 1900 db as those for deep station pairs farther south. Assuming zero net transport below 1900 db between Stas 16 and 19 gives a reference level near 2400 db. That would imply adding 0.1 Sv per 100 db to the transports relative to 2200 db in Table 1. Probably some, possibly all of the reversal of transport at Stas 16–17 and 19 is only apparent, and associated with short period variability of dynamic heights. In the latter case, it may be more appropriate to ignore Sta. 17 and calculate the transport using only Stas 16 and 19. That makes negligible difference to the net transport between those stations, but it has an appreciable effect on the extrapolation to the slope beyond Sta. 19, depending on which

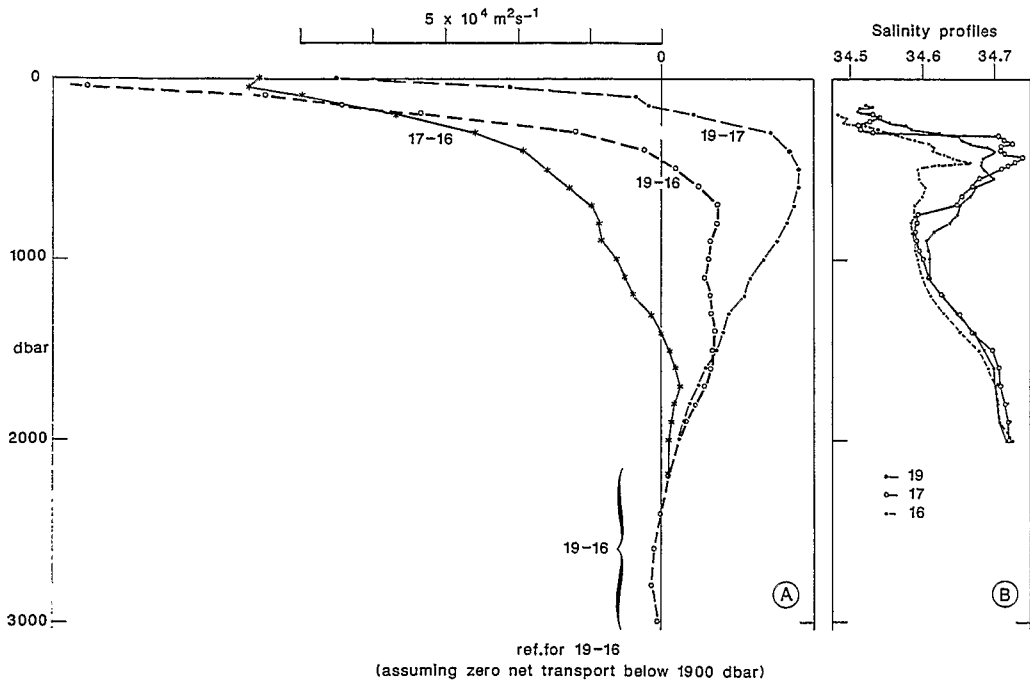


Fig. 15. (a) Variability of the vertical distribution of transport per unit depth between Stas 16, 17 and 19 near the coast of Bali; (b) Corresponding salinity profiles.

Sta. pair, 17-19 or 16-19, is used. In Table 1, the mean of the two extrapolations has been applied.

In an attempt to reduce the noise level on dynamic heights, all the CTD data (two or three casts per station in most cases) for each station on this section have been averaged and interpolated on to a 50 km grid. The dynamic heights have been computed relative to 2200 dbar and the resulting transports are shown in Tables 1 and 2. The vertical distribution of transport is substantially the same as before: 19.1 Sv westward in the top 200

Table 1. Australia-Bali section transports in Sv, reference level 2200 db, including extrapolation to ends and Ekman transport

Layers	Transport in Sv deep casts	Transport in Sv averaged casts, 50 km grid
0-200 db	-23.1	-19.1
200-500 db	-2.7	-3.1
Total 0-500 db	-25.8	-22.2
500-2000 db	+9.6	+6.3
Total 0-2000 db	-16.2	-15.9

Table 2(a). Summary of transports using averaged and interpolated stations on regular 50 km grid (including extrapolation to ends and Ekman transport) and corresponding transport-weighted mean salinity and temperature

σ_θ range	Transport in Sv (+ve eastwards)	mean <i>S</i> (psu)	mean <i>T</i> (°C)	Remarks
<25 (0–167 db mean)	5.5	34.50	24.4	S end–13°36'S
	–20.1	34.12	24.2	13°36'S–N end
	–14.6	33.97	24.1	net values for layer
25–27 (167–533 db)	5.4	34.77	12.7	S end–13°36'S
	–14.1	34.56	12.4	13°36'S–N end (exclud. input to Sumba channel)
	1.2	34.69	8.7	9°56'S–N end. to Sumba channel
	–7.5	34.38	12.7	net values for layer
27–27.5 (533–1280 db)	1.7	34.612	6.3	S end–12°41'S
	–8.0	34.600	5.9	12°41'S–9°56'S
	8.8	34.625	5.9	9°56'S–N end
	2.5	34.70	6.2	net values for layer
27.5–27.7 (1280–1860 db)	1.6	34.661	3.3	S end–10°51'S
	–2.1	34.676	3.4	10°51'S–9°56'S
	3.6	34.682	3.4	9°56'S–N end
	3.1	34.68	3.3	net values for layer
Total (<27.7)	–16.5	33.92	25.6	net values for layer

Table 2(b). Same as Table 2a, if we make minimum adjustments to transports in the two lower layers to make them consistent with salinities in the Bali–Timor section, and reduce inflow to Sumba channel to the observed geostrophic transport in the Bali–Timor section

σ_θ range	Transport in Sv (+ve eastwards)	mean <i>S</i> (psu)	mean <i>T</i> (°C)	Remarks
27–27.5	1.7	34.612	6.3	as in Table 2a
	–8.0	34.600	5.9	as in Table 2a
	1.8	34.625	5.9	entrained into outflow to Sumba channel
	2.8	34.625	5.9	
27.5–27.7	0.6	34.661	3.3	entrained into outflow to Timor channel
	1.0	34.661	3.3	
	–2.1	34.676	3.4	as in Table 2a
	1.5	34.682	3.4	entrained into outflow
adjusted total (<27.7)	–22.8	34.12	19.9	net values for adjusted total

db, including ends and Ekman transport. Below 400 db, weak eastward transport is indicated at all levels. The spatial distribution of transport is summarized in Table 2, subdivided vertically by density surfaces and latitudinally into subsections of net eastward and westward transport. These correspond fairly well, though not always exactly, to the

Table 2(c). Same as Table 2(a), if we leave the 27-27.5 layer unadjusted, and change only the 27.5-27.7 layer as in Table 2(b)

σ_θ range	Transport in Sv (+ve eastwards)	mean S (psu)	mean T (°C)	Remarks
adjusted total (< 27.7)	-18.6	34.00	23.0	net values for alternative adjusted total

distribution of water masses already described. As may be expected, the transport within each subsection can be quite variable, and the uncertainties are large, about ± 2 to ± 4 Sv per subsection, and at least ± 7 Sv for the net transport through the whole section, even using these averaged stations. In the upper two layers, transports are large enough to be significant. A total of 10.9 Sv of mainly subtropical water goes eastwards through the section south of $13^\circ 36'S$. This is presumably all returned westwards in the 34.2 Sv outflow north of that latitude, having mixed with a contribution of 23.3 Sv from the Indonesian seas. In the lower layers, transports are of marginal or no significance, but will be discussed later, together with the rest of Table 2.

Transports through the Bali-Timor section. Along the Bali-Timor trench section, the geopotential topography is very variable (Fig. 16). Several factors may contribute: effects of curvature and other accelerations at the exit from the channels, frictional effects from the irregular bathymetry, the section cutting diagonally across the mouths of some channels and so encountering parts of the along-channel pressure gradients, the presence of relatively strong tidal currents. Much of the variability in Fig. 16 is time-varying: see the changes when Stas 30 and 34 were repeated. The sense of slope, i.e. the direction of the surface current, is unchanged even when the repeated stations are used, though the implied speeds would be reduced by half. Despite the high noise level, it is worth noting that in Fig. 16 there are indications of faster southwestward geostrophic surface currents in the middle of each channel; Sta. pairs 22-23, 25-26, 29-30 and 33-34. Moreover, comparison with Fig. 10a shows that these mid-channel fast currents are associated with lower near-surface salinities, giving more confidence in their existence, though their speed is quite uncertain.

In the central part of the Australia-Bali section, Stas 5-16, transports were changed very little when all the stations were used, compared to using only the deep stations. This encouraged us to try calculating transports in the Bali-Timor section using only the seven stations that go to at least 1700 db, i.e. deeper than all the sill depths except the Timor trench sill. There are of course shallower depths than 1700 db between some station pairs in the section, but there is always deeper water immediately to the southwest, so it seems legitimate to use 1700 db as a reference level. For the last station pair, partly in the Timor trench, a reference level of 1200 db has been used, consistent with the Pegasus profiles and the deep water properties. Estimates of the transport for the whole section, 0-1700 db (Table 3) differ by 9.6 Sv depending on whether Sta. 34 or its repeat Sta. 39 is used in the Timor trench. Despite this large variability, the transports are not inconsistent with those of Table 1 for the Australia-Bali section. Figure 12 shows the similarity of the transports for the two sections.

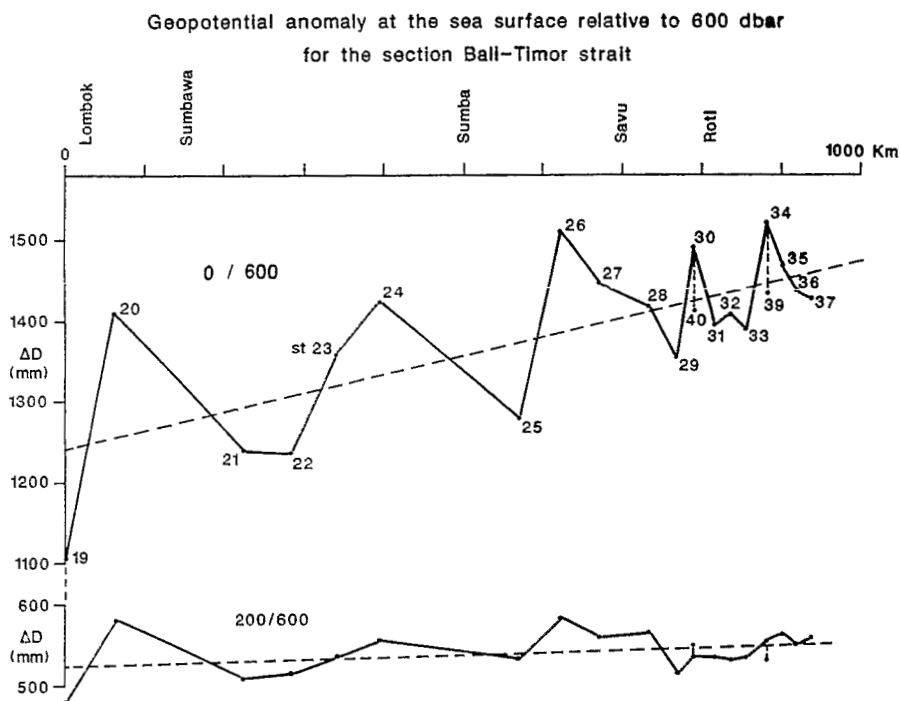


Fig. 16. Geopotential anomaly at the sea surface and at 200 dbar relative to 600 dbar for the section Bali-Timor strait.

Mean salinity and temperature of the throughflow water and salinity constraints. The transports calculated from the averaged stations in the Australia-Bali section relative to 2200 db are thought to be the least uncertain of the estimates given in Table 1. They are presented in subdivided form in Table 2a, together with mean (transport-weighted)

Table 3. Transports for Bali-Timor section using only stations to at least 1700 db

Layer in db	Transport in Sv A	Transport in Sv B
0-200	-26.5	-20.1
200-500	-4.1	-1.7
500-1100	1.3	2.4
1100-1700	2.9	2.7
Total: 0-1700	-26.4	-16.7

A: stations 19, 21, 22, 23, 25, 29 and 34.

B: stations same but with Sta. 39 instead of 34.

Reference level 1700 db except for 29-34 and 29-39 (1200 db). Transports include extrapolation to 200 m contour and Ekman transport (-1.9 Sv) in top layer.

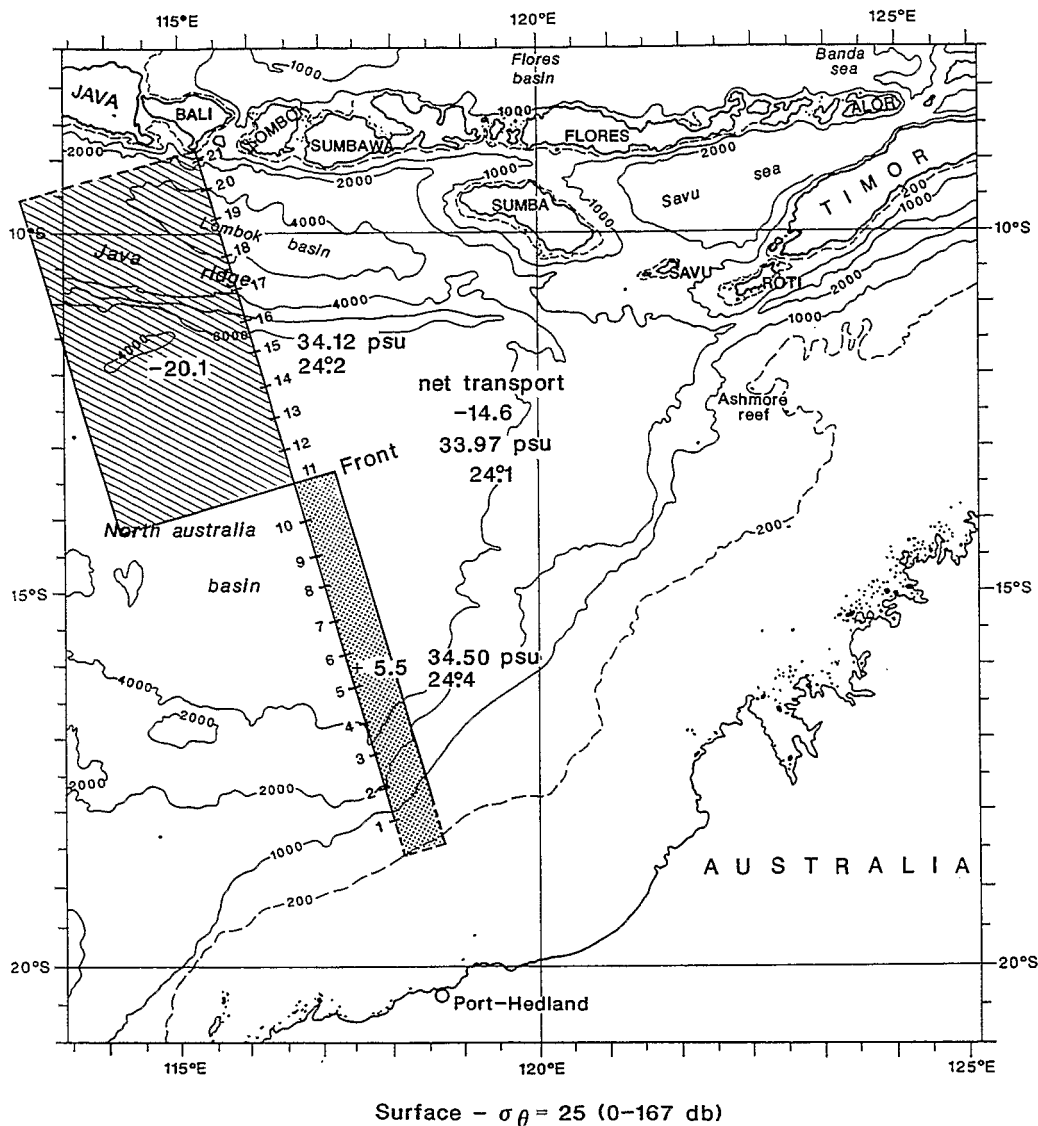


Fig. 17. Spatial distribution of the geostrophic transports between surface and $\sigma_{\theta} = 25$ (0-167 dbar) computed from the averaged stations over a regular grid of 50 km with a reference level of 2200 db (including Ekman transport and extrapolation to 200 m isobath).

salinities and temperatures for each subdivision, and for the net throughflow transport (the transports in the layer $0-\sigma_{\theta} = 25$ is presented on Fig. 17). The net throughflow, 16.5 Sv westward (Table 2a) is warmer and fresher than any of the subdivisions. This comes about because the east-going water at all levels is relatively saline, and much of it is cold. In the upper two layers of Table 2a, attempts to make salinity budgets for the two sections were defeated by the evident unsteadiness of the salinity distribution. A patch of exceptionally low salinity in the density range $25 < \sigma_{\theta} < 26$ at Stas 12-17 in the outflow through the

Australia–Bali section could not have been formed by mixing the southern Indian Ocean water with the water of that density range present in the Bali–Timor section. In the two lower layers, observed salinities are less variable and, where comparisons could be made, are close to historical mean values. This gives some hope that conditions may be steadier there. On the other hand, transports are generally too small to have significance, and the correspondence between the transport subdivisions and water properties is less clearly defined. If, despite the limitations, we attempt to make salinity budgets, we are led to conclude that in both lower layers the estimates of eastward transport of high salinity water at the northern end of the section are too large. Very little of it can be incorporated into the westward outflow, if conditions are steady. Some, but probably not much, can be exported eastwards through the Sumba channel. One possible set of adjusted transports is given in Table 2b, a more modest adjustment in Table 2c. The propriety of making such adjustments may seem questionable at first sight, but Fig. 13 shows that differences in estimates of geostrophic transport of order 5 Sv can occur, spread vertically through the 500–2000 db interval, without necessarily changing the reference level or transports in the rest of the profile.

5. DISCUSSION

Results of the water mass analysis show that, on the deep section, between the Australian continental shelf and Bali, a sharp subsurface front separates the South Indian ocean Subtropical water and the water of the Indonesian Seas of Pacific origin, around 13°30'S below the mixed layer down to 700 m. The south Indian Ocean Subtropical water was not entering the Indonesian seas. Near the coast of Bali, in the surface layer, a strong upwelling appears under the action of the southeast monsoon associated to a strong southwestward current. At depth, around 300–800 m, a water mass of relatively high salinity (>34.7), low oxygen concentration ($<2.0 \text{ ml l}^{-2}$), is found close to the coast. It corresponds to a water mass of northern Indian Ocean origin, the Northern Indian Ocean Water, which is also found off Lombok strait and Sumba strait. The main pathway of the throughflow lies between Bali and the hydrological front at 13°30'S. It is a region of intense mixing with the water coming from the Indonesian seas (Banda sea water) and the water masses coming from the northern and southern Indian Ocean. In the axis of each channel, there is a core of low salinity, high oxygen content from the surface to 50 m corresponding to higher velocities. The Indonesian straits drive intense currents down to the bottom. A reversal of the flow towards the east from 1200 m to the bottom has been detected from current profiles done in the strait. This reversal corresponds to the entrance of the upper part of the Indian Ocean Deep water into the Timor basin.

From the hydrographic data of the deep section between Australia and Bali done during the peak of the southeast monsoon, the geostrophic transports estimated with different reference levels give a mean estimation of the throughflow between 0 and 500 m of $22 \text{ Sv} \pm 4 \text{ Sv}$ towards the Indian Ocean with a concentration of the transport (70%) in the 0–200 m layer and near the Indonesian coast (north of 13°30 S). The estimates of the total transport in the throughflow down to 1900 m (Table 2) have an uncertainty of at least $\pm 7 \text{ Sv}$. If we have to choose a single value, the 18.6 Sv of Table 2c seems preferable, with corresponding mean salinity of 34.0 psu and temperature 23°C. From the three-cast stations, part of the short term variability has been estimated. The uncertainty on the geostrophic transports comes mostly from that short term variability. Below 1900 m, which is below the deepest

sill anyway, the estimated geostrophic transports are within the noise level. To get the complete throughflow transport, measurements of the transport on the Australian continental shelf must be included. An estimation has been done by CRESSWELL *et al.* (1993) using different kinds of direct current measurements which amounts to approximately 1 Sv westwards.

The values for the net transport and mean salinity of the throughflow (Table 2), fall between two previously published estimates. PIOLA and GORDON (1984) obtained a transport of 10–14 Sv with a mean salinity of 33.0–33.6 psu. WIJFFELS *et al.* (1992), assuming a mean salinity of 34.5 psu, deduced a mass transport for the throughflow of $31.5 \times 10^9 \text{ kg s}^{-1}$, which they recognized as much too large. Changing their mean salinity to 33.9–34.1 psu (Table 2) would give mass transports $14.3\text{--}17.5 \times 10^9 \text{ kg s}^{-1}$, or 14–17 Sv, not significantly different from our 18.6 ± 7 Sv. There are several reasons why our estimate may be higher than average. First, it was estimated from one section made at the height of the southeast monsoon which is the season where the transport must be the highest (see the different models results). Second, it was estimated from measurements done at the end of a “La Nina” event (i.e. stronger southeast trade winds over the equatorial Pacific and higher precipitations over the “maritime continent”), whereas the other two studies, being based on large-scale freshwater budgets, yield climatological mean estimates.

Acknowledgements—We are very grateful to our colleagues in getting the data during the cruise: M. A. Foujols, C. Levy, J. Lanoisellé, J. M. Janin, A. Poisson and his team of LPCM; N. Metzl, B. Schauer, B. Bres, C. Brunet, E. Cohen-Solal, N. Poisson, B. Ollivier from the TAAF and L. Gamberoni who helped in the calibration of the CTD data.

We are much indebted to the Terres Australes et Antarctiques Françaises for their efficient support to carry out the JADE 1989 cruise. The help of the Scientific Attaché of the French Embassy in Jakarta has been particularly appreciated. We recognize the great support of L. Merlivat. We thank Klaus Schulze, who works at the University of Hamburg under the leadership of D. R. Quadfasel, for bringing a Pegasus profiler which allowed to get an important information on the current profile. The critical comments of a reviewer have been most helpful.

These results on the throughflow would not have been possible without the cooperation between French and Indonesian scientists. We would like to convey our thanks to the BPPT in Indonesia and particularly Professor M. T. Zen for organizing such a fruitful cooperation.

REFERENCES

- BROECKER W. S., W. C. PATZERT, J. R. TOGGWEILER and M. STUIVER (1986) Hydrography, chemistry and radioisotopes in the southeast Asian basins. *Journal of Geophysical Research*, **91**, (C12), 14,345–14,354.
- BULLISTER J. L. and R. F. WEISS (1988) Determination of CCl_3F and CCL_2F_2 in seawater and air. *Deep-Sea Research*, **35**, 839–853.
- COX M. (1982) *Numerical models of ocean circulation*. National Academy Press, Washington D.C.
- CRESSWELL G. R., A. FRISCHE, J. PETERSON and D. QUADFASSEL (1993) Inter-ocean throughflow in the Timor sea. *Journal of Geophysical Research*, **98**, C8, 14379–14389.
- FIEUX M., A. KARTAVTSEFF and A. G. ILAHUDE (1990) Recueil des données de la campagne MD 62/JADE. Vol. 1: *Hydrologie*. Rapport interne TAAF-LODYC-BPPT-LIPI.
- FINE R. (1985) Direct evidence using tritium data for the throughflow from the Pacific into the Indian Ocean. *Nature*, **315**, 478–480.
- FU L. (1986) Mass, heat and freshwater fluxes in the south Indian Ocean. *Journal of Physical Oceanography*, **16**, 1683–1693.
- GODFREY J. S. and T. J. GOLDING (1981) The Sverdrup relation in the Indian Ocean, and the effect of Pacific-Indian Ocean throughflow on Indian Ocean circulation and on the east Australian current. *Journal of Geophysical Research*, **11**, 771–779.
- GODFREY, J. S. and A. J. WEAVER. Is the Leeuwin current driven by Pacific heating and winds? *Progress in Oceanography* (submitted).

- GORDON A. (1986) Inter-ocean exchange of thermocline water. *Journal of Geophysical Research*, **91**, 5037–5046.
- HELLERMAN S. and M. ROSENSTIEN (1983) Normal monthly wind stress over the World Ocean with error estimates. *Journal of Physical Oceanography*, **13**, 1093–1104.
- KINDLE J. C., G. W. HEBURN and R. C. RHODES (1987) An estimate of the Pacific to Indian Ocean throughflow from a global numerical model. In: *Further progress in equatorial oceanography*, E. J. KATZ and J. M. WITTE, editors, Nova University Press, Fort Lauderdale, pp. 317–321.
- KINDLE C., H. E. HURLBURT and E. J. METZGER (1989) *Seasonal and interannual variability of the Pacific to Indian ocean throughflow*, J. PICAUT, R. LUCAS and T. DELCROIX, editors, Proceedings of the western Pacific international meeting and workshop on TOGA COARE, Noumea.
- MANTISI F. (1989) Perspectives quant à la pénétration du CO₂ anthropique. Utilisation des fréons 11 et 12 comme traceurs des masses d'eaux océaniques dans l'océan Indien Sud Ouest. Thèse de Doctorat en Océanologie de l'Université Paris 6, 3 mai 89, 178 pp.
- MCCARTNEY M. S. (1977) Subantarctic Mode Water. In: *A voyage of discovery*, M. V. ANGEL, editor. *Deep-Sea Research*, **24** (Supplement), 103–119.
- MOLCARD R., J. BANJARNAHOR, M. FIEUX and A. G. ILAHUDE. Low frequency variability of the currents in Indonesian straits.
- MURRAY S. P. and D. ARIEF (1988) Throughflow into the Indian Ocean through the Lombok Strait, January 1985–January 1986. *Nature*, **333**, 444–447.
- MURRAY S. P., D. ARIEF, J. C. KINDLE and H. E. HURLBURT (1990) Characteristics of circulation in an Indonesian Archipelago strait from hydrography, current measurements and modeling results. In: *The physical oceanography of sea straits*, L. J. PRATT, editor, pp. 3–23.
- PALMER T. N. and D. A. MANSFIELD (1986) A study of winter time circulation anomalies during past El Niño events using a high resolution GCM. Part II: variability of the seasonal mean response. *Quarterly Journal of the Royal Meteorological Society*, **112**, 639–660.
- PHILANDER G. (1990) *El Niño, La Niña and the Southern oscillation*. International Scientific Series, **46**, 293 pp. Academic Press, San Diego, California.
- PIOLA A. R. and A. L. GORDON (1984) Pacific and Indian Ocean upper-layer salinity budget. *Journal of Physical Oceanography*, **14**, 747–753.
- QUADFASSEL D. R. and G. CRESSWELL (1992) A note on the seasonal variability of the south Java current. *Journal of Geophysical Research*, **97** (C3), 3685–3688.
- ROCHFORD D. J. (1966) Distribution of Banda intermediate water in the Indian Ocean. *Australian Journal of Marine and Freshwater Research*, **17**, 1–30.
- ROCHFORD D. J. (1969) Seasonal variations in the Indian Ocean along 110°E. I. Hydrological structure of the upper 500 m. *Australian Journal of Marine and Freshwater Research*, **20**, 1–50.
- RICHARDSON P. and T. K. MCKEE (1989) *Surface velocity in the Equatorial Oceans (20N–20S) Calculated from Historical Ship Drifts*. WHOI technical report, April 89.
- SEMTNER A. J. JR. and R. M. CHERVIN (1988) Global Ocean Circulation with Resolved Eddies. *Journal of Geophysical Research*, **C12**, 15,502–15,522.
- SVERDRUP H. U., M. W. JOHNSON and R. H. FLEMING (1942) *The oceans: their physics, chemistry and general biology*. Prentice-Hall, New Jersey, 1087 pp.
- TOOLE J. M., E. ZOU and R. C. MILLARD (1988) On the circulation of the upper waters in the western equatorial Pacific Ocean. *Deep-Sea Research*, **35**(9), 1451–1482.
- VAN AKEN H. M., J. PUNJANAN and S. SAIMIMA (1988) Physical aspects of the flushing of the east Indonesian basins. *Netherlands Journal of Sea Research*, **22**(4), 315–339.
- WARREN B. A. (1981a) Transindian hydrographic section at Lat. 18°S: Property distributions and circulation in the South Indian Ocean. *Deep-Sea Research*, **28**, 759–788.
- WARREN B. A. (1981b) Note on the shallow oxygen minimum of the South Indian Ocean. *Deep-Sea Research*, **28**, 859–864.
- WUFFELS S. E., R. W. SCHMITT, H. L. BRYDEN and A. STIGEBRANDT (1992) Transport of freshwater by the oceans. *Journal of Physical Oceanography*, **22**(2), 155–162.
- WYRTKI K. (1961) *Scientific Results of Marine Investigation of the South China Sea and the Gulf of Thailand*. NAGA Report 2. University of California
- WYRTKI K. (1971) *Oceanographic Atlas of the International Indian Ocean Expedition*, NSF, 531 pp, Washington.
- WYRTKI K. (1987) Indonesian throughflow and the associated pressure gradient. *Journal of Geophysical Research*, **92**, C12, 12,941–12,946.